Journal Pre-proof

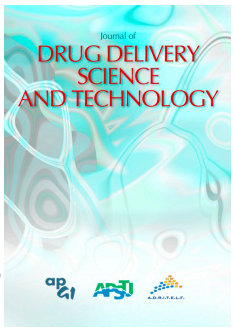

Anticancer activity of NFκB decoy oligonucleotide-loaded nanoparticles against human lung cancer

Vinod Kumar Kannaujiya, Gabriele De Rubis, Keshav Raj Paudel, Bikash Manandhar, Dinesh Kumar Chellappan, Sachin Kumar Singh, Ronan MacLoughlin, Gaurav Gupta, Dia Xenaki, Pradeep Kumar, Philip Michael Hansbro, Brian Gregory George Oliver, Peter Richard Wich, Kamal Dua

PII: S1773-2247(23)00180-6

DOI: https://doi.org/10.1016/j.jddst.2023.104328

Reference: JDDST 104328

To appear in: *Journal of Drug Delivery Science and Technology*

Received Date: 20 November 2022

Revised Date: 28 February 2023

Accepted Date: 2 March 2023

Please cite this article as: V.K. Kannaujiya, G. De Rubis, K.R. Paudel, B. Manandhar, D.K. Chellappan, S.K. Singh, R. MacLoughlin, G. Gupta, D. Xenaki, P. Kumar, P.M. Hansbro, B.G.G. Oliver, P.R. Wich, K. Dua, Anticancer activity of NFκB decoy oligonucleotide-loaded nanoparticles against human lung cancer, *Journal of Drug Delivery Science and Technology* (2023), doi: https://doi.org/10.1016/j.jddst.2023.104328.

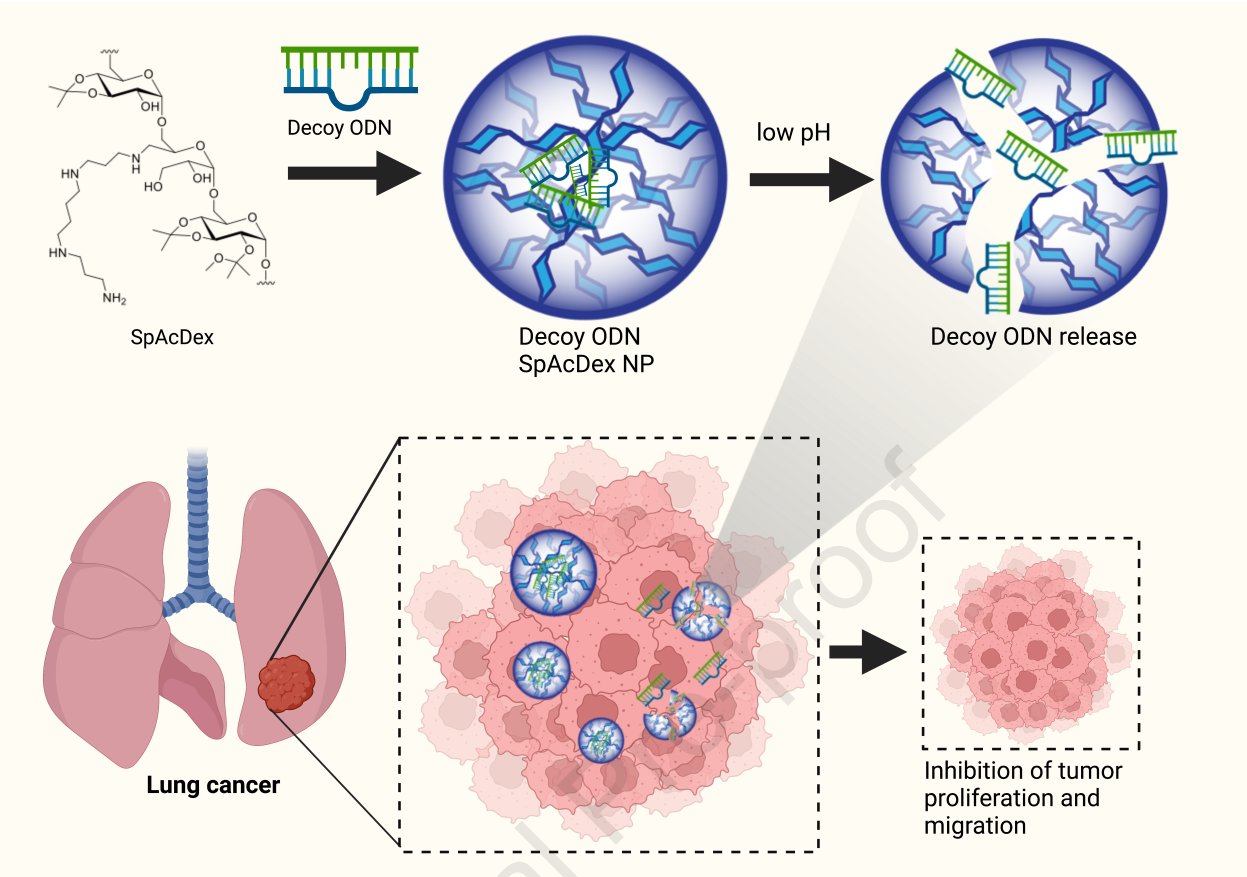

Anticancer activity of NFκB decoy oligonucleotide-loaded nanoparticles against human lung cancer

Vinod Kumar Kannaujiya[1,2#], Gabriele De Rubis[3,4#], Keshav Raj Paudel[5], Bikash Manandhar[3,4], Dinesh Kumar Chellappan[6], Sachin Kumar Singh[4,7], Ronan MacLoughlin[8,9,10], Gaurav Gupta[11,12], Dia Xenaki[13], Pradeep Kumar[14], Philip Michael Hansbro[5,15], Brian Gregory George Oliver[13,15*], Peter Richard Wich[1,2*], Kamal Dua[3,4,*]

[1] School of Chemical Engineering, University of New South Wales, Sydney, NSW 2052, Australia

[2] Australian Centre for NanoMedicine, University of New South Wales, Sydney, NSW 2052, Australia

[3] Discipline of Pharmacy, Graduate School of Health, University of Technology Sydney, Sydney, NSW 2007, Australia

[4] Faculty of Health, Australian Research Centre in Complementary and Integrative Medicine, University of Technology Sydney, Ultimo, NSW 2007, Australia

[5] Centre for Inflammation, Centenary Institute and University of Technology Sydney, Faculty of Science, School of Life Sciences, Sydney, NSW 2007, Australia

[6] Department of Life Sciences, School of Pharmacy, International Medical University, Bukit Jalil 57000, Kuala Lumpur, Malaysia

[7] School of Pharmaceutical Sciences, Lovely Professional University, Jalandhar-Delhi GT Road, Phagwara 144411, Punjab, India

[8] IDA Business Park, H91 HE94 Galway, Connacht, Ireland

[9] School of Pharmacy & Biomolecular Sciences, Royal College of Surgeons in Ireland, D02 YN77 Dublin, Leinster, Ireland

[10] School of Pharmacy & Pharmaceutical Sciences, Trinity College, D02 PN40 Dublin, Leinster, Ireland

[11] School of Pharmacy, Suresh Gyan Vihar University, Jaipur 302017, Rajasthan, India

[12] Uttaranchal Institute of Pharmaceutical Sciences, Uttaranchal University, Dehradun 248007, Uttarakhand, India

[13] Woolcock Institute of Medical Research, University of Sydney, Sydney, New South Wales, Australia

[14] Wits Advanced Drug Delivery Platform Research Unit, Department of Pharmacy and Pharmacology, School of Therapeutic Sciences, Faculty of Health Sciences,

University of the Witwatersrand, Johannesburg, South Africa

[15] School of Life Sciences, University of Technology Sydney, Ultimo, NSW 2007, Australia

[#] These two authors contributed equally to this work

* Corresponding Authors: Kamal Dua (kamal.dua@uts.edu.au); Peter Richard Wich (p.wich@unsw.edu.au); Brian Gregory George Oliver (brian.oliver@uts.edu.au).

Abstract (200-300 words)

Non-small cell lung cancer (NSCLC) is among the leading global causes of cancer-related mortality. Current treatment options have limited efficacy and severe adverse effects, underlining the necessity for innovative therapeutic strategies. Among emerging strategies, NFκB inhibition is particularly promising, as NFκB is considered a master regulator of NSCLC pathogenesis. NFκB activity can be efficiently inhibited by double-stranded decoy oligodeoxynucleotides (ODNs). However, therapeutic use of ODNs is strongly limited by enzymatic degradation and poor transport across cell membranes. In this study, we report the encapsulation of a small hydrophilic NFκB decoy ODN into a biodegradable, biocompatible, and acid-responsive dextran-based nanoparticle (NP) system. This formulation has shown excellent encapsulation efficiency (up to 99.5%) with 185 nm average particle size and pH-dependent ODN release at acidic pH. NFκB decoy ODN NPs showed promising anticancer activity, with significant anti-proliferative, anti-migratory, and anti-colony formation activity. These were measured by MTT assay, Boyden chamber and scratch wound healing assays, and crystal violet staining, respectively. Mechanistically, the anti-proliferative effect was exerted through the activation of the expression of key genes regulating apoptosis and necroptosis such as TNF-α, RIPK1, RIPK3, and MLKL. The findings of this study provide the foundations for further investigation of the molecular mechanisms by which NFκB inhibition results in anticancer activity, simultaneously providing proof-of-concept of the therapeutic potential of dextran-based nanoparticles carrying NFκB decoy ODNs against NSCLC.

Keywords: AcDex nanoparticles, decoy oligodeoxynucleotides, lung cancer, NSCLC, migration, proliferation, NFκB, pulmonary delivery

Graphical abstract

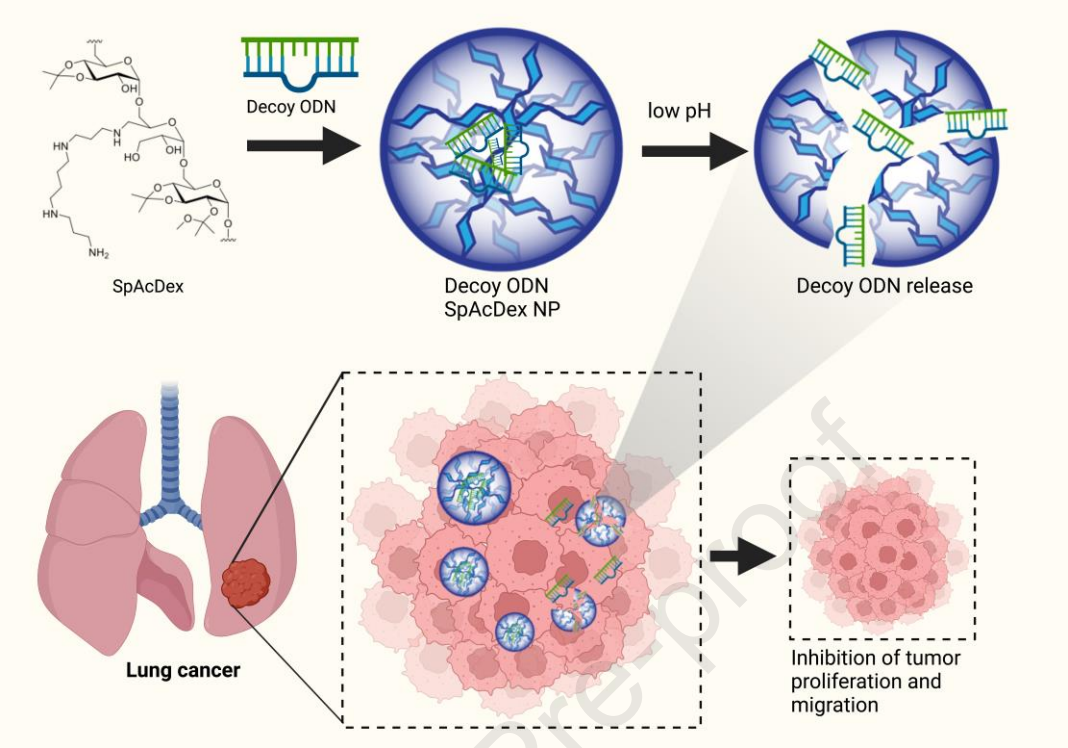

Image created with BioRender.com

1. Introduction

Across all cancer types, lung cancer (LC) is one of the leading causes of death, with more than 1.7 million LC-related deaths recorded in the world in 2020 [1]. Non-small-cell lung cancer (NSCLC) represents the majority (85%) of LC cases [2]. The five-year survival rate of LC is only 17.8%, lower than that of other main cancers [3]. Besides smoking, other factors causing LC include increasing urbanization and environmental pollution [4].

The current mainstay treatment modalities for LC include surgery [5], chemotherapy [6], radiotherapy [7], targeted therapy [8], and immunotherapy [9, 10]. Despite the availability of numerous treatment strategies, a large percentage of patients experience relapse and treatment resistance [9]. This, together with the elevated chemo- and radiation toxicity associated to chemotherapy and radiotherapy [11], demonstrates the urgency for the development of innovative NSCLC treatment strategies with increased efficacy and reduced toxicity [12-14].

Nuclear factor κB (NFκB) represents a family of transcription factors that was discovered in 1987 as factors binding to the enhancer of k immunoglobulins in activated B cells [15]. Since then, NFκB has been found to have a pivotal role in the transcriptional regulation of a plethora of cellular responses, particularly related to the immune system and inflammation [16]. Besides its role in the immune response, NFκB is an essential contributor to many cancer hallmarks, as its activation promotes phenomena such as tumour cell proliferation and survival [17], and it is considered the key point of connection between persistent infections, chronic inflammation, and increased cancer risk [18]. In NSCLC, NFκB is considered a master regulator of cancer pathogenesis and progression, influencing many aspects of this cancer such as proliferation [19], cancer survival, [20], cancer cell migration, infiltration and metastasis [21], and epithelial-to-mesenchymal transition (EMT) [22]. Recently, increased NFκB expression in NSCLC was associated with reduced overall survival and 5-year survival rate, worsening tumour stage, and lymph node metastasis [23]. This supports the potential of targeting and inhibiting NFκB as an effective approach for LC therapy [24, 25], and numerous molecules inhibiting the NFκB pathway are currently being studied [26]. Despite this, no NFκB targeting treatment has reached clinical approval for application as cancer therapy.

Among the many possible modalities of NFκB inhibition for therapeutic purposes, the use of decoy oligodeoxynucleotides (ODNs) represents a viable strategy [27, 28]. Decoy ODNs are therapeutic molecules consisting in double-stranded synthetic oligonucleotides with a sequence that mimics the DNA target sequence of the intended transcription factor. As a consequence,

the transcription factor binds specifically to the decoy ODN, and fewer copies of the transcription factor are available to bind the target DNA, resulting in the net inhibition of the transcription factor's activity [29]. For this reason, decoy ODNs represent promising tools to finely regulate the activity of specific transcription factors in many diseases [30, 31]. In a recent study, for example, the transfection with a NFκB decoy ODN resulted in strong suppression of the proliferation of the androgen-independent prostate cancer cell line PC-3M, together with induction of apoptosis [32]. Despite the versatility of decoy ODNs, these therapeutic tools have many limitations, including lack of tissue specificity in the case of systemic administration [33] and, importantly, an unfavourable pharmacokinetic profile [27] characterised by two major issues: (1) low cellular permeability due to the large size and presence of negative charges; and (2) instability of the ODN under *in vivo* conditions due to nuclease activity [34]. This results in reduced therapeutic efficacy [27, 35, 36]. Despite structural ODN modifications such as peptide nucleic acids (PNAs) [37], locked nucleic acids (LNAs) [38] and phosphorothioate-substituted ODNs [33] resulted in increased resistance to degradation, concerns about toxicity, side effects, poor binding efficacy and specificity of these nucleotide derivatives remain [27]. For this reason, there is a need to develop suitable delivery systems for NFκB decoy delivery to the target site of action [39].

One potential strategy to efficiently deliver ODN cargo to target cells is represented by the use of advanced nanocarriers allowing pulmonary delivery through nebulization [40]. *De Rosa et al* have reported a biodegradable polymer, poly(DL-lactic *co*-glycolic acid) (PLGA)-based micro spherical particle, for the delivery of NFκB decoy ODN in RAW 264.7 macrophages, obtaining sustained release of ODN together with inhibition of NFκB at low concentrations [41]. Similarly, NFκB ODN-loaded PLGA microspheres were reported to achieve site-specific delivery of ODN in a rat-carrageenin sponge implant model, inhibiting NFκB activation in chronic inflammation [42].

Polysaccharide-based drug delivery systems have gained a considerable interest due to properties such as biocompatibility, biodegradability, and easy chemical modification [43, 44]. Recently, NFκB/p65 antisense oligonucleotide-loaded chitosan-based nanoparticles (NPs) were reported to achieve an excellent loading efficiency exploiting ionic interactions between cationic chitosan and anionic nucleotides [45]. Similarly, *Cohen et al* have reported an acid-responsive acetalated dextran-based nanocarrier for the delivery of siRNA to HeLa-luc cells [46]. Upon cellular uptake, the acetal groups undergo hydrolysis under slightly acidic environments such as those found in lysosomes/late endosomes and, importantly, in the tumour

131 microenvironment [47]. This generates water-soluble dextran material, acetone, and methanol
132 as side product [48]. The hydrolysis of the acetal groups initiates the disassembly of NPs and
133 the controlled release of the payload [49]. Additionally, the dextran side chain was modified
134 with spermine to introduce cationic moieties in the polymer, thus facilitating encapsulation of
135 highly polyanionic siRNA molecules through electrostatic interactions. Furthermore, the
136 cationic nature of spermine-modified acetalated dextran (SpAcDex) NPs has shown enhanced
137 cellular uptake due to the electrostatic interactions occurring with the negatively charged cell
138 membrane [50].

139 In this study, we encapsulated NFκB double-stranded decoy ODNs into SpAcDex NPs and
140 evaluated the anticancer activity of this formulation in the human A549 NSCLC cell line. The
141 present study is the first in which an NFκB decoy ODN is encapsulated within a bio-
142 compatible, acid-responsive delivery system, which allows selective release of the payload in
143 the acidic tumor microenvironment. This has the potential to minimize adverse effects caused
144 by the off-target, aspecific inhibition of NFκB in healthy cells. The formulation revealed a
145 strong anticancer activity, with significant inhibition of cancer hallmarks including cancer cell
146 proliferation, migration, and ability to form clonal colonies. Mechanistically, the anti-
147 proliferative effect of this formulation was achieved by enhancing the expression of genes
148 mediating apoptosis and necroptosis such as tumor necrosis factor-α (TNF-α), Receptor-
149 interacting serine/threonine-protein kinases 1 and 3 (RIPK1, RIPK3), and Mixed lineage kinase
150 domain-like (MLKL). This study provides proof-of-concept of the suitability of SpAcDex NP-
151 based ODN formulations for the therapeutic inhibition of NFκB in NSCLC.

152

2. Materials and Methods

2.1 Materials

Dextran (Mw 9-11 kDa, from *Leuconostoc mesenteroides*) was purchased from (Sigma Aldrich). Sodium periodate, 2-Methoxy propene, spermine, Sodium borohydride were purchased from Merck. Water used during particle preparation was adjusted to pH 8 with triethylamine (Sigma Aldrich). All buffers and water used for the preparation of SpAcDex-based NPs were in nuclease free and filtrated through syringe filters (Millex, sterile PES membrane, pore size 0.22 µm, Merck). Brandson Digital Sonifier 450 (Power: 400 watts; Line Voltage: 200-245 @ 50/60 Hz, Consonic Tip Micro Tapered 1/8). Dynamic light scattering (DLS) (Malvern Zetasizer Nano ZS). NFκB decoy ODN and Scramble decoy ODN were purchased from Merck, Bayswater, VIC, Australia MTT (3-[4,5-dimethylthiazol-2-yl]-2,5-diphenyl tetrazolium bromide), crystal violet, DMSO, H/E staining solutions Dulbecco's Modified Eagle's Medium (DMEM), fetal bovine serum (FBS), and penicillin and streptomycin were purchased from Sigma-Aldrich, St. Louis, MO, USA. All remaining agents and solvents used in experiments involving cell culture were purchased from Sigma-Aldrich unless stated otherwise.

2.2 Synthesis of Spermine-Functionalized Acetalated Dextran

The spermine-functionalized acetalated dextran was synthesized over three steps according to literature [46].

Partial Oxidation of Dextran (OxDex): For the synthesis of partially oxidized dextran, dextran (2.0 g, 12.3 mmol) was dissolved in 8.0 mL dd-H_2O. The solution was stirred for 5 h at room temperature after sodium periodate (480 mg, 2.25 mmol) addition. Further, the reaction mixture was dialyzed against dd-H_2O for 3 days using a snakeskin regenerated cellulose membrane with MWCO of 3,500 g/mol. After lyophilization, a colourless powder (1.3 g) was obtained, with an aldehyde content of 8.9 ± 0.02 mol aldehyde per 100 mol anhydrous glucose units (AGU) confirmed by BCA assay.

Acetalation of Partially Oxidized Dextran (OxAcDex): The solubility switch from hydrophilic to hydrophobic dextran was obtained as described by *Bachelder et al*. The oxidized dextran (1 g, 6.17 mmol) was dissolved in DMSO (12.0 mL). Further, 2-methoxypropene (2.6

g, 36 mmol) was added slowly after addition of pyridinium *p*-toluenesulfonate (22 mg, 0.088 mmol). The reaction mixture was stirred for 10 min at room temperature followed by reaction quenching with the help of triethylamine (1 mL) [48]. The resulting reaction mixture was precipitated in dd-H_2O pH 8 (100 mL) and isolated by centrifugation (12,000 g, 20 min, 4 °C). The product was further washed 5 times with dd-H_2O pH 8. After lyophilization, the OxAcDex (1.2 g) was obtained as a colorless powder. The obtained product contains 79.1% acetals, where 30.2% are cyclic and 48.9% are acyclic acetals.

Spermine Modification of OxAcDex (SpAcDex): To further modify oxidized acetalated dextran with spermine, the Ox-AcDex (1.0 g, (AGU) 202 g/mol, 5.05 mmol) was dissolved in DMSO (4.5 mL). After addition of spermine (1 g, 5.05 mmol), the reaction mixture was incubated with continuous stirring for 24 h at 40 ºC. Afterwards, sodium borohydride (560 mg, 15.2 mmol) was added, and reaction was stirred for additional 24 h at 50 ºC. After purification using similar method as mentioned above, the product was lyophilized to obtain a white powder. The degree of functionalization was determined by elementary analysis (1.36% N, 53.46% C and 7.83% H) and resulted in 4.8 mol spermine per 100 mol AGU.

2.3 Transcription Factor Decoy ODN

Single stranded decoy ODN to double stranded NFκB inhibitor was obtained by annealing. The sequence of sense and antisense oligodeoxynucleotides was annealed in 1×annealing buffer (20 mM Tris-HCl, 20 mM $MgCl_2$ and 50 mM NaCl, pH 7.5). The mixture was heated at 80 ºC for 5 min and allowed to cool slowly at room temperature overnight.

The sequence of the ODN decoy to NFκB used was:

(1) NFκB decoy ODN sequence

5’-CCTTGAAGGGATTTCCCTCC-3’

3’-GGAACTTCCCTAAAGGGAGG-5’

(2) scrambled decoy ODN sequence

5’-TTGCCGTACCTGACTTAGCC-3’

3’-AACGGCATGGACTGAATCGG-5’

2.4 Nanoparticle Preparation

ODN-loaded and empty nanoparticles were prepared by a double emulsion method using a probe sonicator. 10 mg spermine-modified acetalated dextran was dissolved in 800 μL dichloromethane (DCM) and 130 μL phosphate-buffered saline (PBS) with and without 121.5 μg annealed ODN was added for loaded and empty nanoparticle formulations, respectively. The first sonication was performed for 10 second followed by addition of 4 mL polyvinyl alcohol (PVA) solution (3% w/w in PBS, 13–27 kDa, 87–89% partially hydrolyzed) on top of primary emulsion. Further, a second sonication was performed for 30 s to achieve a secondary water-in-oil-in-water emulsion. The resulting emulsion was stirred overnight to allow DCM evaporation followed purification by ultracentrifugation (45,000 x g, 20 min, 20 °C) and was washed three times with 4.0 mL dd-H_2O (pH 8). Before lyophilization, 50 μL PVA solution (0.3% w/w in dd-H_2O pH 8) was added as cryoprotectant. The particle yield was about 60%, based on the initial spermine-modified dextran material.

2.5 Measurement of Particle Size and Zeta Potential

The size of the different dextran-based NP was determined by nanoparticle dynamic light scattering (DLS), using a Malvern Zetasizer Nano ZS. All NP samples were measured in dd-H_2O (pH 8.0) after sonication (Unisonics FXP) for 60 s at 25 °C in triplets. The size calculation was performed with Malvern software. Zeta potential (particle charge) was measured using a clear disposable zeta cell. Three measurements with 20 individual runs each were performed at 25 °C. Particle samples were prepared at concentrations of 0.1 mg/mL in HEPES buffer (25 mm, pH 7.4). The calculation was performed with the Malvern Zetasizer software 6.20. Data shown represent the average zeta potential (standard deviation of distributions of three sequential measurements).

2.6 Scanning Electron Microscopy (SEM)

Particle shape and morphology were analyzed by scanning electron microscopy (SEM). The freeze-dried Dex(ODN-loaded) NPs dispersed in distilled (1 mg^{-1}·mL) were dried and coated with Pt layer under argon atmosphere. Images of the samples were taken on an FEI Nova Nano SEM 230 FE-SEM at an accelerating voltage of 5.0 kV.

2.7 Determination of ODN Loading by RiboGreen Assay

An indirect method of quantification was performed to determine the encapsulated double-stranded decoy ODN in double emulsion particles using the Quant-iT™ RiboGreen® assay [51]. Here, particle solution was centrifuged after particle formation and solvent evaporation. The amount of free decoy ODN present in the supernatant was then quantified and compared with the initial concentration of decoy ODN used in particle formulation [52]. The non-encapsulated decoy ODN present in the supernatant was able to react with the RiboGreen® reagent resulting in a fluorescent compound with an emission maximum at 535 nm (λex = 485 nm). To determine the decoy ODN content, 10 µL of the supernatant was combined with 90 µL of PBS in a black, flat-bottom 96-well microplate. Meanwhile, the pure double-stranded decoy ODN was diluted in PBS to a concentration that ensured 100% encapsulation. The RiboGreen® reagent was diluted 1:200 with PBS, and 100 µL was added to each well, resulting in a total volume of 200 µL per well. The reaction mixture was then carefully incubated for 5 minutes in the dark before the fluorescence of the reacted dye was recorded using a Tecan microplate reader. To further verify any presence of free decoy ODN in the nanoparticle pellets, the particles were washed twice with nuclease free pH 8.0 water and ODN content were measured in supernatant. The results were compared with the fluorescence of the theoretical amount of encapsulated decoy ODN using Microsoft Excel to determine total ODN loading. Loading content and encapsulation efficiency was calculated according to formula as LC and EE.

$$\text{LC (wt \%)} = \frac{\text{weight of ODN in particle}}{\text{weight of ODN-loaded particle}} \cdot 100\% \qquad \textbf{eq. 1}$$

$$\text{EE (wt \%)} = \frac{\text{weight of ODN in particle}}{\text{weight of total ODN used in particle formulation}} \cdot 100\% \qquad \textbf{eq. 2}$$

2.8 pH-Dependent Degradation of SpAcDex Particles

Empty particles were suspended in triplicate at a concentration of 0.25 mg/mL in either a 0.3 M acetate buffer (pH 5.5) or PBS (pH 7.4) buffer and incubated at 37 ºC under gentle agitation

using a MultiTherm shaker (Eppendorf). At various time points, the size distribution of the samples was measured using DLS. For visual observation, the particles were incubated at a concentration of 2.5 mg/mL and were photographed at various time points.

2.9 pH-Dependent Release of Decoy ODN from SpAcDex Particles

ODN-loaded particles were incubated at a concentration of 5 mg/mL in either a 0.3 M acetate buffer (pH 5.5) or PBS (pH 7.4) buffer at 37 ºC temperature under gentle agitation using a thermo incubator (Eppendorf). At different time interval the aliquots were collected and centrifuged at 10 000g for 10 min to pellet out insoluble materials, and the supernatant was stored at -20 ºC. The release ODN in the supernatant sample was quantified by Quant-iT™ RiboGreen® assay. The amount of ODN in each sample was calculated by fitting the emission to a calibration curve using the Quant-iT™ RiboGreen® assay. For this experiment, all solutions included heparin at 25 mg/mL to disrupt electrostatic interactions between polymer amines and decoy ODN to enable quantification.

2.10 ODN Molecular Generation and Visualization

The double stranded molecular structures of NFκB and scrambled ODNs were generated using the default DNA/RNA builder tool in Avogadro 2.0.8.0 Molecule Editor & Visualizer System [53]. The generated ODN structure was then visualized and scanned using UCSF Chimera 1.14 Molecular Modelling System employing conventional Nucleic Acid Database (NDB) colors and formats [54].

2.11 Cell Culture

A549 (human lung epithelial carcinoma) and BEAS-2B (human non-cancerous bronchial epithelial) cell lines (ATCC, USA) were a kind gift from Prof. Alaina Ammit, Woolcock Institute of Medical Research, Sydney, Australia. Cells were cultured in DMEM supplemented with 10% FBS, 1% penicillin and streptomycin, in a humified 37°C incubator supplied with 5% CO_2.

2.12 Cell Viability Assessment - MTT Assay

The MTT assay was performed to assess A549 and BEAS-2B cell proliferation and viability as previously described [55, 56]. Briefly, 5000 A549 cells/well were seeded in a 96-well plate and, 24 hours post attachment, cells were treated with Dex(NFκB-ODN) NPs or Dex(scrambled-ODN) NPs or empty nanoparticles at different concentrations (corresponding to 0.5, 1, 2.5, 5, 10 nM ODN). Twenty-four hours after treatment, MTT solution (20 µL of a 5 mg/mL stock solution MTT in PBS, for a final concentration of 0.5 mg/mL MTT) was added to the wells and the mixture was incubated at 37 °C for 4 hours. Successively, the supernatant was removed and 100 µL dimethyl sulphoxide (DMSO) were added to each well to dissolve the formazan crystals. The absorbance of the wells was then read using an UV/VIS spectrophotometer at a wavelength of 540 nm. The percent viability of the cells treated with either Dex(NFκB-ODN) NPs or Dex(scrambled-ODN) NPs or empty NPs was reported as percentage compared to the control (untreated) group.

2.13 Wound Healing Assay

The wound healing assay was performed as reported previously [57-59] to assess the anti-migratory activity of the Dex(NFκB-ODN) NPs on A549 cells. Briefly, $3*10^5$ A549 cells/well were seeded into 6-well plates and cultured until confluency. The cell monolayer was scratched using the tip of a sterile 200 µL pipette tip, followed by multiple washing steps with PBS. Images at 0 hr time point were taken after PBS washing, then A549 cells were treated with 10 nM Dex(NFκB-ODN) NPs or concentration-matched Dex(scrambled-ODN) NPs for 24 hours. The distance between the edges of the scratch before and 24 h after treatment was measured using the IS capture software after imaging with a light microscope at 10X magnification, and the percentage wound closure was reported compared to the control (untreated) group.

2.14 Boyden's Chamber Assay

To determine A549 cells migration, a modified Boyden's chamber assay was performed as previously described [58, 60], using transwell permeable supports (6.5-mm insert 8-µM pore size polycarbonate membrane). First, the lower surface of the membranes was coated with 2.5% gelatin in 1M acetic acid for 1 hour. Subsequently, cells were seeded in the upper chamber at a density of 10^4 cells/mL in a volume of 200 µL DMEM culture media. The chamber was

328 then placed in a well containing 600 µL DMEM. After attachment, the cells were treated with
329 10 nM Dex(NFκB-ODN) NPs or concentration-matched Dex(scrambled-ODN) NPs for 24h,
330 and cells were allowed to migrate for 24 hours more after the end of the treatment. Following
331 this, the non-migrated cells remaining in the upper surface of the membrane were removed
332 using cotton swabs, while the cells that successfully migrated reaching the lower surface were
333 fixed in 10% formalin and stained with hematoxylin and eosin. Finally, the cells that had clearly
334 migrated through the pores of the membranes were counted in 5 random fields with a light
335 microscope, with a 20x magnification. Average cells per field of view were then calculated and
336 reported.

337

338 **2.15 Colony Formation Assay**

339 The colony formation assay was performed as reported previously [58, 61] to test the anti-
340 colony formation activity of Dex(NFκB-ODN) NPs in A549 cells. First, cells were seeded at a
341 density of 500 cells/well into six-well plates. Following adhesion, cells were treated with 10
342 nM Dex(NFκB-ODN) NPs or concentration-matched Dex(scrambled-ODN) NPs. After colony
343 development (about 2 weeks), the cells were washed with PBS and fixed with 3.7%
344 formaldehyde for 20 minutes. Successively, cells were washed again with PBS and stained
345 with 0.4% crystal violet, then washed four to five times with PBS. The colonies were finally
346 counted using the ImageJ software.

347

348 **2.16 Real-time qPCR**

349 The effects of Dex(NFκB-ODN) NPs on the mRNA expression levels of proliferation-related
350 genes were assessed through quantitative real-time PCR (qPCR) as described in a previous
351 study [61]. First, $1.5*10^5$ A549 cells/well were seeded into 6-well plates and left to attach
352 overnight. The following day, cells were treated with 10 nM Dex(NFκB-ODN) NPs or
353 concentration-matched Dex(scrambled-ODN) NPs for 24 h. After the treatment, the cells were
354 lysed with 500 µL TRI reagent (Sigma-Aldrich, Australia). The samples were vortexed for 45
355 seconds to ensure complete cell rupture. Successively, 125 µL chloroform (Sigma-Aldrich,
356 Australia) were added and the samples were centrifuged at 12,000 g, 3°C, for 15 minutes. The
357 aqueous layer was transferred into fresh tubes and the RNA was precipitated by adding 250 µL
358 ice-cold isopropyl alcohol (Sigma-Aldrich, Australia). The tubes were then centrifuged at

12,000 g, 3°C, for 10 min. After centrifugation, the supernatant was removed, and the precipitated RNA pellets were washed twice with 1 mL 75% ethanol (Sigma-Aldrich, Australia), centrifuging the tubes at 8,000 g, 4 °C, for 5 min each time. After the second centrifugation, the ethanol was removed, and dried RNA pellets were dissolved in 20 µL nuclease-free water (Sigmal-Aldrich, Australia). Nanodrop (Thermo Fisher Scientific, Waltham, MA, USA) was used to determine the concentration and purity of the RNA samples.

The RNA samples were subjected to DNase I (Sigma-Aldrich, Australia) treatment. Successively, 800 ng total RNA was reverse-transcribed to cDNA using the reaction mixture of M-MLV buffer (Thermo Fisher Scientific), random primers (0.5 µg/µL, Thermo Fissher Scientific), dNTPs (10 mM, Thermo Fisher Scientific) and DTT (100 mM, Thermo Fisher Scientific). For the reverse transcription reaction, a thermal cycler (Eppendorf, Hamburg, Germany) was used with the following steps: denaturation (65 °C, 10 min), annealing (25 °C, 10 min), reverse transcription (37 °C, 50 min), and enzyme inactivation (70 °C, 15 min). An amount of 16 ng of cDNA from each sample was then subjected to real-time qPCR using the iTaq Universal SYBR green (BioRad, Hercules, CA, USA) mix and gene-specific primers (forward and reverse, 0.5 µM each, Sigma-Aldrich, Australia). The thermal cycler used was a CFX96 PCR system (BioRad). The real-time qPCR protocol included the following cycles: 95 °C for 30 s (1 cycle), 95 °C for 15 s (50 cycles) and 60 °C for 30 s (1 cycle). The human gene for Glyceraldehyde 3-phosphate dehydrogenase (GAPDH) has been used as a control for normalization.

The sequences of human primers used were as follows:

Gene name	**FW sequence**	**RV sequence**
TNF-α	AGGCAGTCAGATCATCTTC	TTATCTCTCAGCTCCACG
RIPK1	TGATAATACCACTAGTCTGACG	ACAGTTTTTCCAGTGCTTTC
RIPK3	AACTTTCAGAAACCAGATGC	GTTGTATATGTTAACGAGCGG
MLKL	GTGAAGAATGTGAAGACTGG	AAGATTTCATCCACAGAGGG
GAPDH	TCGGAGTCAACGGATTTG	CAACAATATCCACTTTACCAGAG

2.17 Statistical Analysis

The data are represented as mean ± SEM. Statistical analysis was performed by ordinary one-way ANOVA, followed by Tukey multiple comparison test. The software used was GraphPad Prism (v.9.4, GraphPad Software, San Diego, CA, USA). In pairwise comparisons, a two-tailed p-value <0.05 was considered statistically significant. In Figure 4d, a Mann-Whitney U test was performed between the 5nM and 10 nM Dex(NFκB)

3. Results

3.1 Nanoparticle Size and Zeta Potential

The obtained NPs were visualized and characterized by dynamic light scattering (DLS, **Figure 1a**) and scanning electron microscopy (SEM, **Figure 1b**). The spherical morphology of the NPs was confirmed by SEM data. Both empty and double stranded decoy ODN loaded particles have shown similar particle diameter distribution, in the range of 150 to 200 nm. A slight increase in the particle size distribution was observed in loaded particles compared to empty particles. The surface charge of the particles was determined by zeta-potential measurements (***Table 1***). A positive surface zeta-potential of 12.43 mV was observed for empty nanoparticles due to the presence of protonated amines on the particle surface. The encapsulation of the charged decoy ODN slightly reduced the surface zeta potential (11.83-12.37 mV) which is most likely due to the non-covalent adsorption of a small number of negatively charged decoy ODN on the surface of particles.

Molecular modelling was used to predict the three-dimensional structure of the ODNs, which demonstrated self-assembly into well-defined tubular structures with acidic phosphate groups forming the periphery of the tubular structure and amine groups aligning in the centre (**Figure S1)**. This is important for efficient encapsulation and loading of the ODNs into spermine-AcDex nanosystems, wherein the amines of the cationic polymer interact with the negatively charged peripheral phosphate groups of the ODNs [62].

Table 1: *Physical Characterization of empty, NFκB ODN and scramble ODN loaded Dex NP*

Particle Type	Diameter (nm)	PDI	Zeta-Potential / mV
Dex(empty) NP	178 ± 1.0	0.20 ± 0.01	12.4 ± 0.5
Dex(NFκB-ODN) NP	187 ± 1.5	0.23 ± 0.01	11.8 ± 0.3
Dex(scramble-ODN) NP	182 ± 6.0	0.24 ±0.03	12.4 ± 0.5

(The data obtained from three replicate DLS measurements are represented as the mean ± standard deviation)

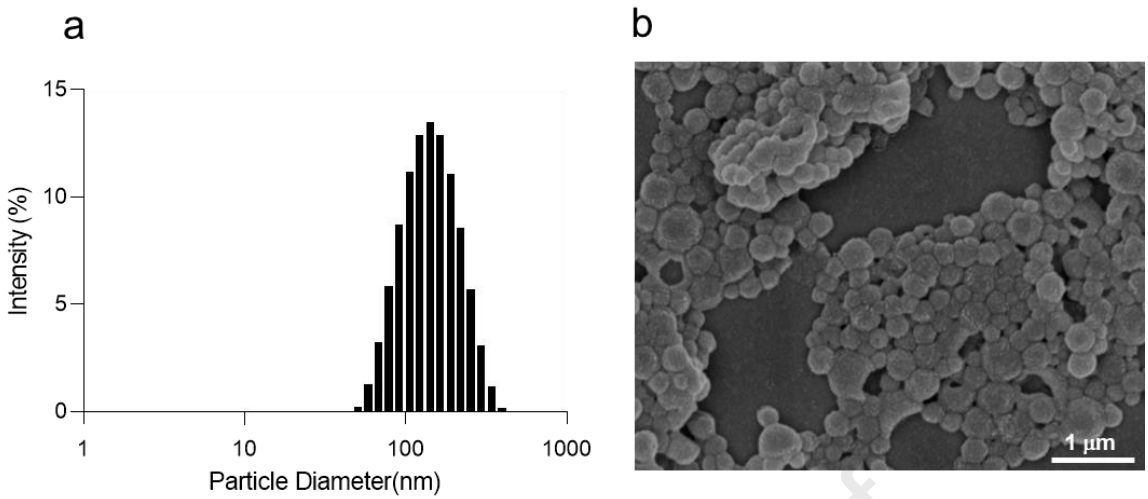

Figure 1. Characterisation of decoy ODN-Encapsulated dextran NPs. *(a) Size distribution obtained by DLS; (b) SEM analysis.*

3.2 Quantification of Decoy ODN Loading

An indirect method of quantification was performed to validate the successful encapsulation and quantification of decoy ODN loading [52] using the Quant-iT™ RiboGreen assay. The unloaded decoy ODN present in the supernatant was quantified after centrifugation followed by particle formulation and solvent evaporation. The amount of decoy ODN present in the supernatant represent the total amount of free decoy ODN, which has not been encapsulated in the particles. As the decoy ODN is highly soluble in water, any unencapsulated decoy ODN would stay in the supernatant. Furthermore, the particle pellets were washed twice with pH 8.0 nuclease-free water and a negligible amount of free decoy ODN was observed in the supernatant, providing confirmation of the successful encapsulation of the decoy ODN. Both NFκB and scrambled decoy ODN have shown a similar encapsulation efficiency of up to 99.5%. Overall, up to 11.89 µg decoy ODNs were encapsulated per mg NPs, as shown in **Table 2**.

433 ***Table 2.*** *Quantification of Decoy ODN Encapsulation*

Particle type	Decoy ODN in $\mu g \cdot mg^{-1}$ NP	Encapsulation efficiency (in %)
Dex(NFκB-ODN) NP	11.89	99.5
Dex(scrambled-ODN) NP	11.88	99.4

434

435 **3.3 pH-dependent Particle Degradation**

436 The decoy ODN was encapsulated into an acid-responsive NPs to prevent the premature release
437 of payload under physiological conditions. Under acidic conditions, the acetal groups present
438 on the SpAcDex backbone undergo rapid hydrolysis, forming a water-soluble dextran, acetone
439 and methanol that leads to particle degradation. To determine the degradation behaviour, the
440 NPs were incubated at 37 °C in PBS buffer at pH 7.4 to simulate the physiological conditions
441 of the blood stream and in acetate buffer at pH 5.5 to mimic the acidic tumour
442 microenvironment. The successful pH-dependent particle degradation at acidic pH was
443 confirmed by DLS measurements (**Figure 2**a). The initial increase in particle size (calculated
444 according to number distribution) can be explained by the uncontrolled aggregation of
445 degradation materials and has been observed previously in similar polysaccharide-based
446 nanosystems [63, 64] . The degradation can also be detected by visually observing the particle
447 solutions (**Figure 2**b). While the typical nanoparticular opaqueness clears under acidic
448 conditions, there was no significant change observed in PBS buffer pH 7.4, indicating the
449 stability of the formulation under physiological conditions.

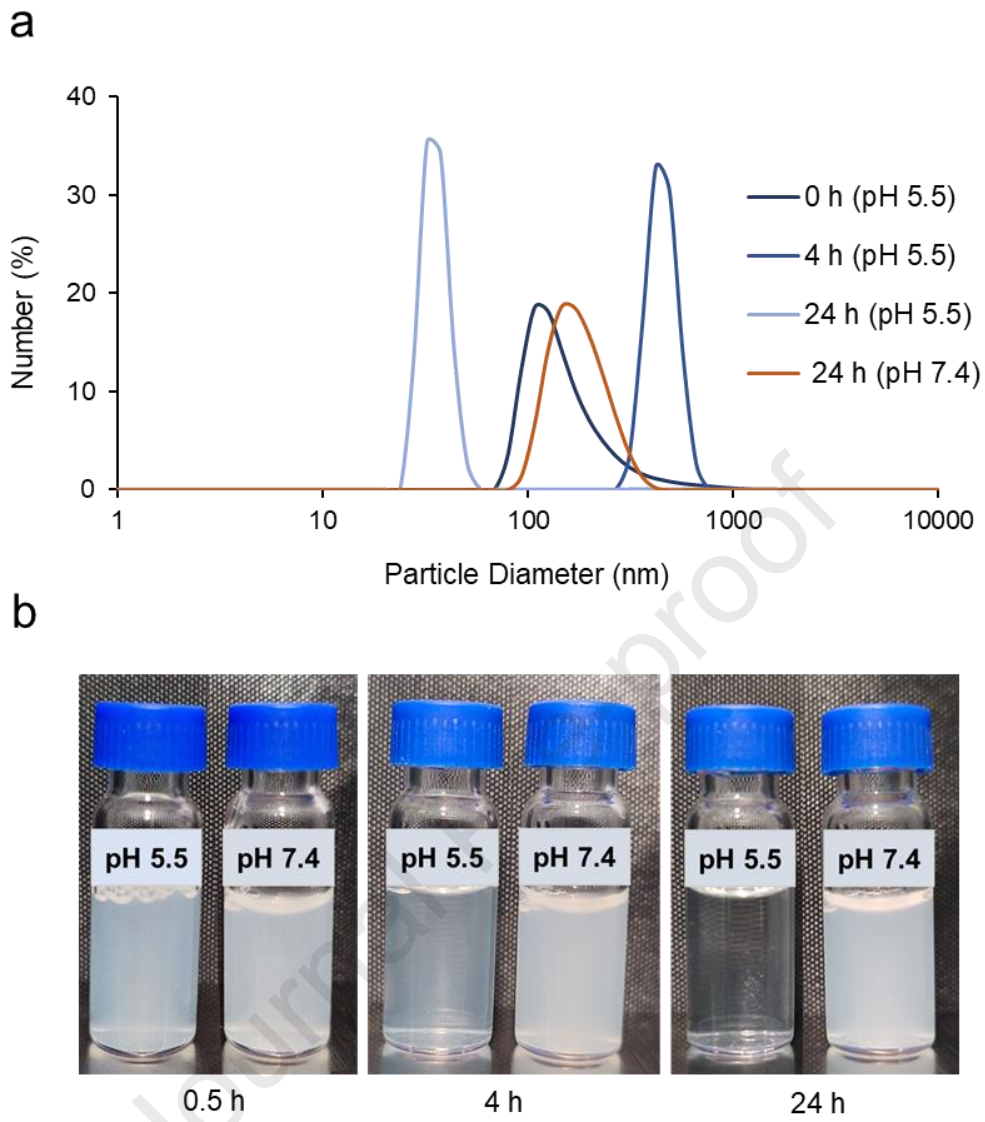

Figure 2. Particle degradation under pH 5.5 and pH 7.4 *(a) DLS data; (b) visual observation.*

3.4 pH-dependent Decoy ODN Release

The decoy ODN-loaded particles were incubated at different pH values similar to the above experiment. The amount of ODNs released from dextran NPs were quantified by using a Quant-iT™ RiboGreen® assay. Heparin was used to prevent the electrostatic interactions between water soluble spermine modified dextran and negatively charged ODN. As expected, a fast release of decoy ODN up to 90% was observed within the first 8 h under acidic conditions [46], while physiological pH 7.4 has shown only a slight release of ODN even after 24 h (**Figure 3**). In the first 5 min after incubation, almost 10% ODN release was observed under both

conditions, indicating the adsorption of free ODN on the surface of particles due to electrostatic interaction between particle surface amine and ODN during formulation.

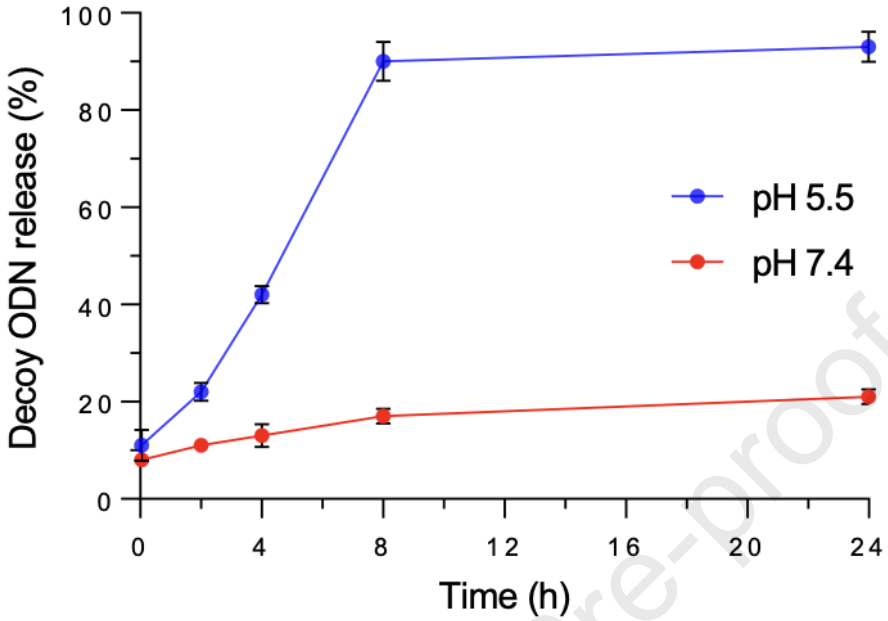

Figure 3. Decoy ODN release under pH 5.5 and pH 7.4 *(Data are presented as means ± SD (n = 3))*

3.5 Anti-proliferative Activity of NFκB-ODN-NPs in A549 and BEAS-2B Cells

The effect of Dex(NFκB-ODN) NPs, Dex(scrambled-ODN) NPs, and empty NPs on the proliferation and viability of A549 and BEAS-2B cells is shown in **Figure 4**. Dex(NFκB-ODN) NPs at concentrations of 2.5, 5 and 10 nM significantly reduced the proliferation rate of A549 cells by 13.4%, 27.8% and 37.2%, respectively, compared to control (untreated cells) in the MTT assay (**Figure 4**a). Considering that the highest anti-proliferative effect was observed with 10 nM Dex(NFκB-ODN) NPs, this concentration has been used for the subsequent experiments. In comparison, treatment with the Dex(scrambled-ODN) NPs at 10 nM concentration resulted only in a relatively small reduction of cell viability of 12% (**Figure 4**b). To assess the effect of Dex(NFκB-ODN) NPs on the viability of non-cancerous cells, the nanoparticles were tested on BEAS-2B human bronchial epithelial cells. Dex(NFκB-ODN) NPs at concentrations of 1, 2.5, 5 and 10 nM significantly reduced the viability of BEAS-2B cells by 8.5%, 14.3%, 15.1%, and 19.2%, respectively, compared to control (untreated cells)

in the MTT assay (**Figure 4d**). The effect of 5nM and 10 nM Dex(NFκB-ODN) NPs on BEAS-2B cell viability was significantly lower than the effect obtained by the same concentration of NPs on A549 cells proliferation (**Figure 4d),** indicating the relative safety of these NPs for healthy cells compared to cancer cells. Treatment with Dex(scrambled-ODN) NPs did not result in a significant reduction of BEAS-2B cell viability (**Figure 4e**). Finally, treatment with empty Dex NPs resulted in no significant effect on A549 and BEAS-2B cell viability at concentrations ranging between 0.5 and 10 µg/mL (**Figures 4c and 4f**, respectively).

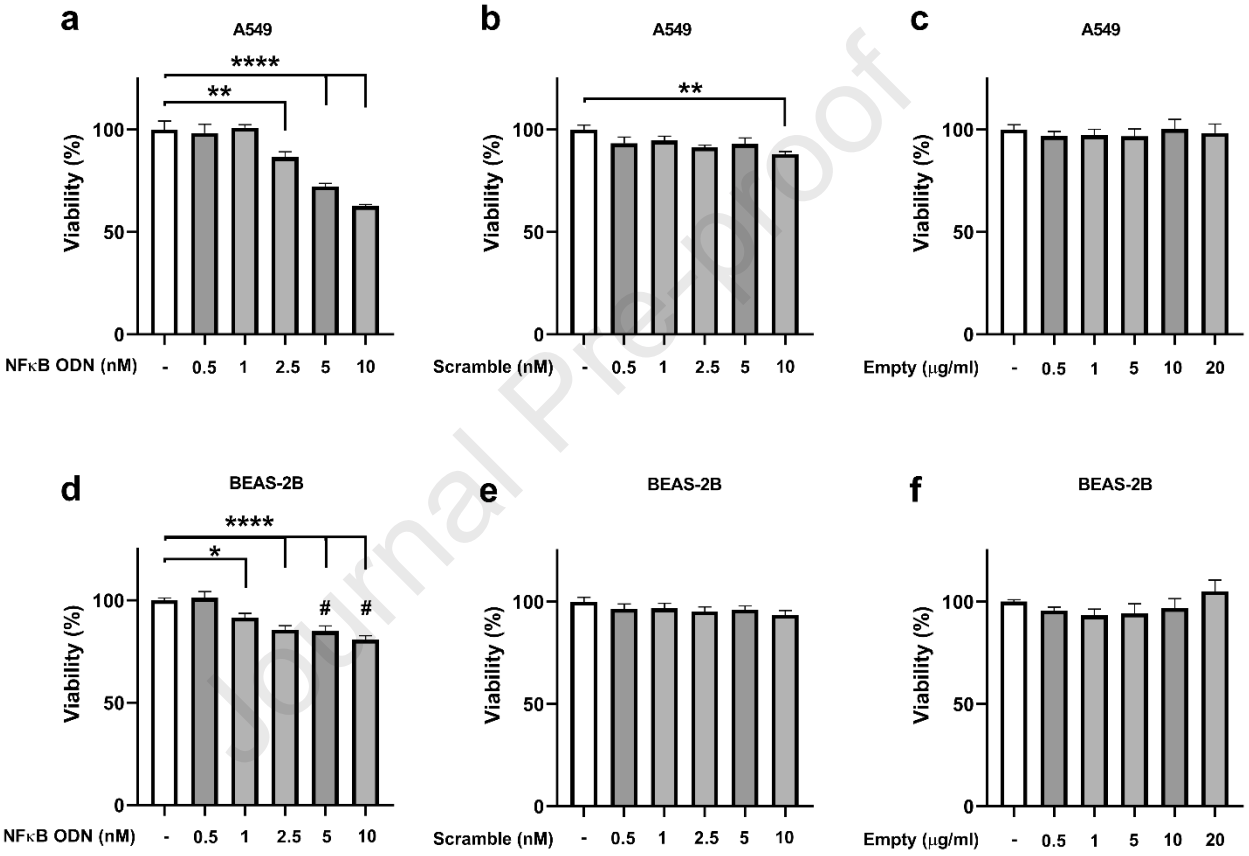

Figure 4. Anti-proliferative activity by MTT assay*: The A549 cells (a-c) and BEAS-2B cells (d-f) were treated with various doses of Dex(NFκB-ODN) NPs (a, d) or Dex(scrambled-ODN) NPs (b, e) or empty NPs (c, f) for 24 hours. The values are expressed as average ± SEM of n = 3 independent experiments. Statistical analysis was performed by ordinary one-way ANOVA test. * = P < 0.05; ** = P < 0.01; **** = P < 0.0001 vs control (untreated). In (d), # = P<0.05 vs concentration-matched group on A549 cells as assessed by Mann-Whitney U test.*

3.6 Effect of Dex(NFκB-ODN) NPs on the expression of apoptosis/necroptosis genes in A549 Cells

To provide a mechanistic explanation of the anti-proliferative effects of Dex(NFκB-ODN) NPs on A549 cells, the effect of the nanoparticle formulation on the expression of transcripts encoding for TNF-α, RIPK1, RIPK3, and MLKL was assessed via real-time qPCR (**Figure 5**). Dex(NFκB-ODN) NPs at 10 nM concentration induced a significant increase in the expression of RIPK1 (11.3%, **Figure 5a**) and MLKL (10.8%, **Figure 5b**). A similar trend was observed with the expression of TNF-α and RIPK3, which was induced on average by 4.9-fold (TNF-α, **Figure 5c**) and 7.1-fold (RIPK3, **Figure 5d**) upon treatment with 10 nM Dex(NFκB-ODN) NPs, without reaching statistical significance. Treatment with Dex(scramble-ODN) NPs did not result in an increase of the expression of any of the four genes analysed (**Figure 5a-d**).

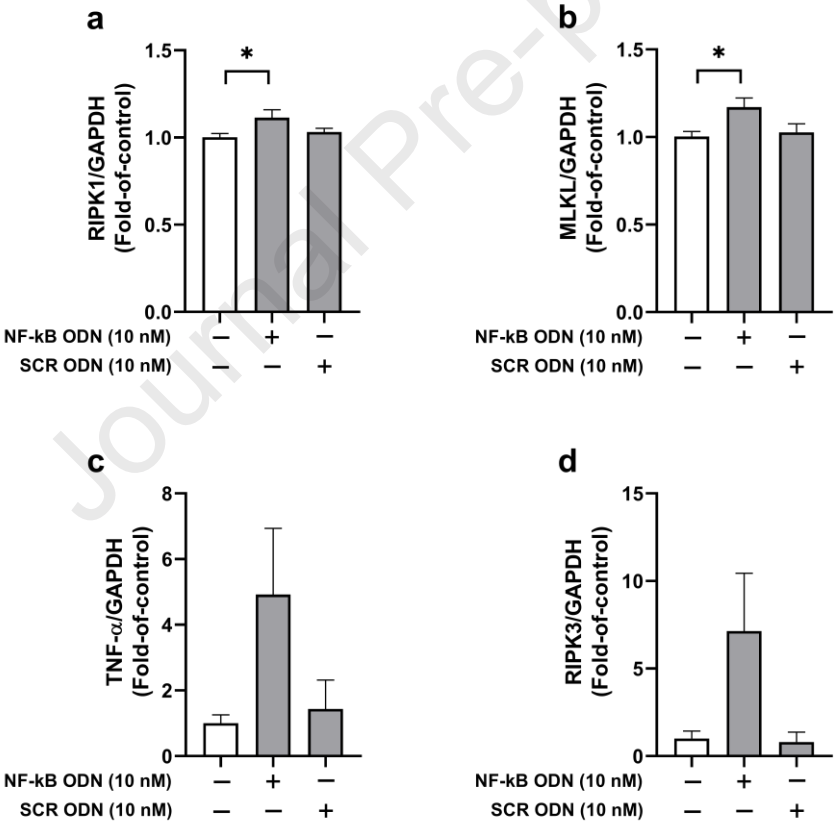

Figure 5. Effect of Dex(NFκB-ODN) NPs on the expression of apoptosis/necroptosis genes in A549 cells. *A549 cells were treated with 10 nM Dex(NFκB-ODN) NPs or Dex(Scramble-ODN) NPs and the relative expression of the following genes was measured with real-time qPCR: RIPK1 (a), MLKL (b), TNF-α(c), and RIPK3 (d). Values are expressed as average ±*

*SEM of n = 3 independent experiments. Statistical analysis was performed by ordinary one-way ANOVA test * = P < 0.05 vs control (untreated).*

3.7 Anti-migratory Activity of NFκB-ODN-NPs in A549 Cells

The effect of Dex(NFκB-ODN) NPs on the migration of A549 cells was assessed by a wound healing assay (

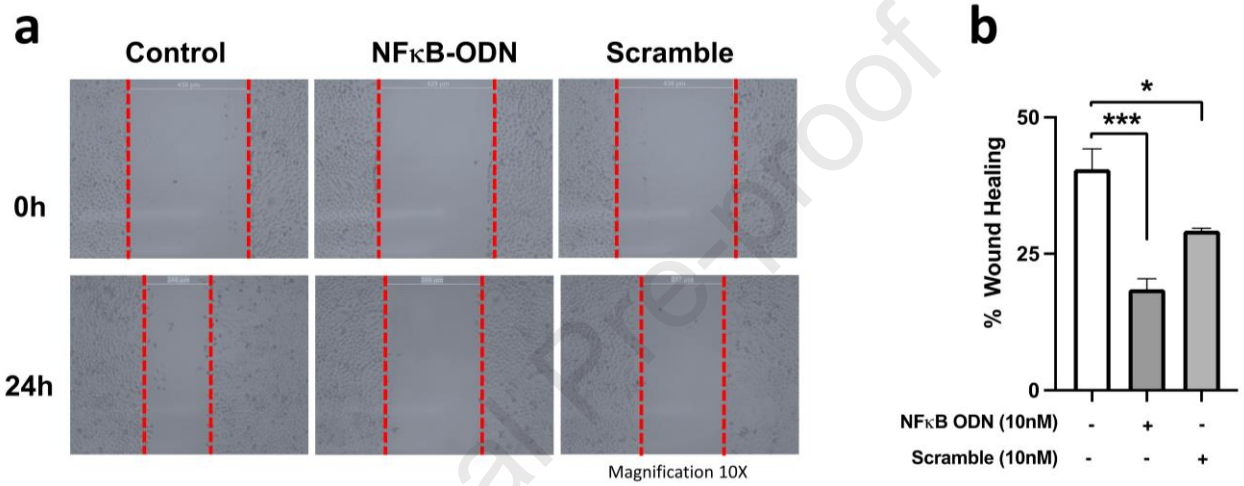

Figure) and by a Boyden chamber assay (**Figure**). Dex(NFκB-ODN) NPs successfully suppressed A549 cell migration in the wound healing assay for 24 h. This treatment has shown 54.3% of migration inhibition compared to the untreated control (

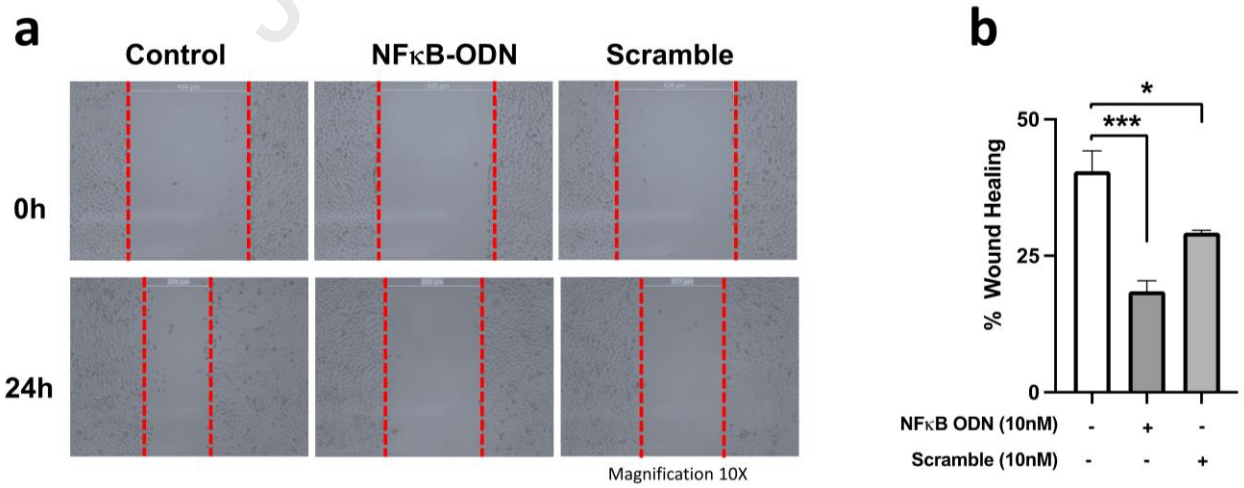

Figure a) while the treatment with similar concentration of Dex(scrambled-ODN) NPs has also somewhat suppressed A549 cells migration, although to a lesser extent compared to the Dex(NFκB-ODN) NPs (27.8% compared to untreated control,

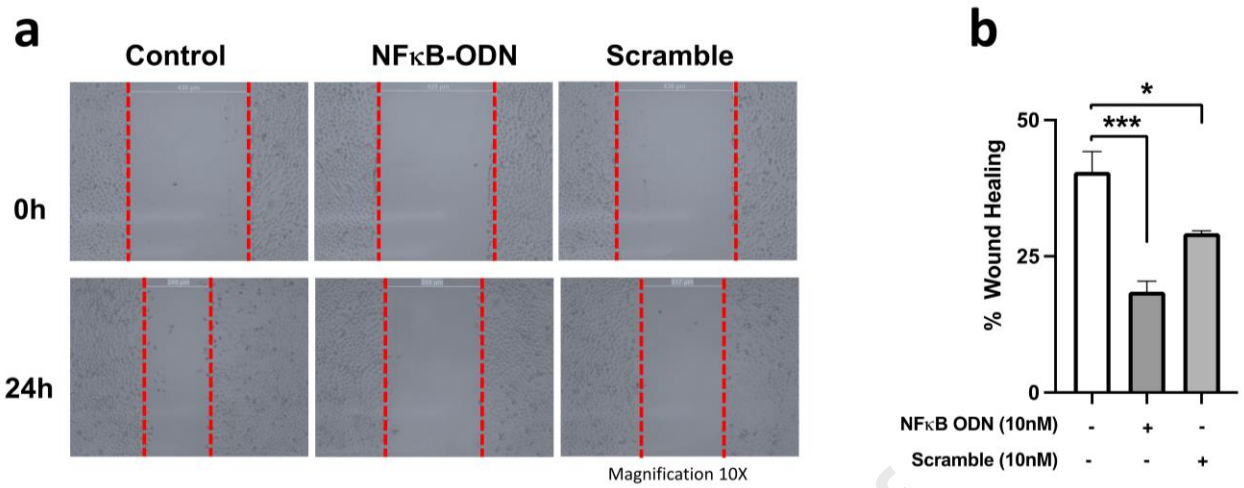

Figure b).

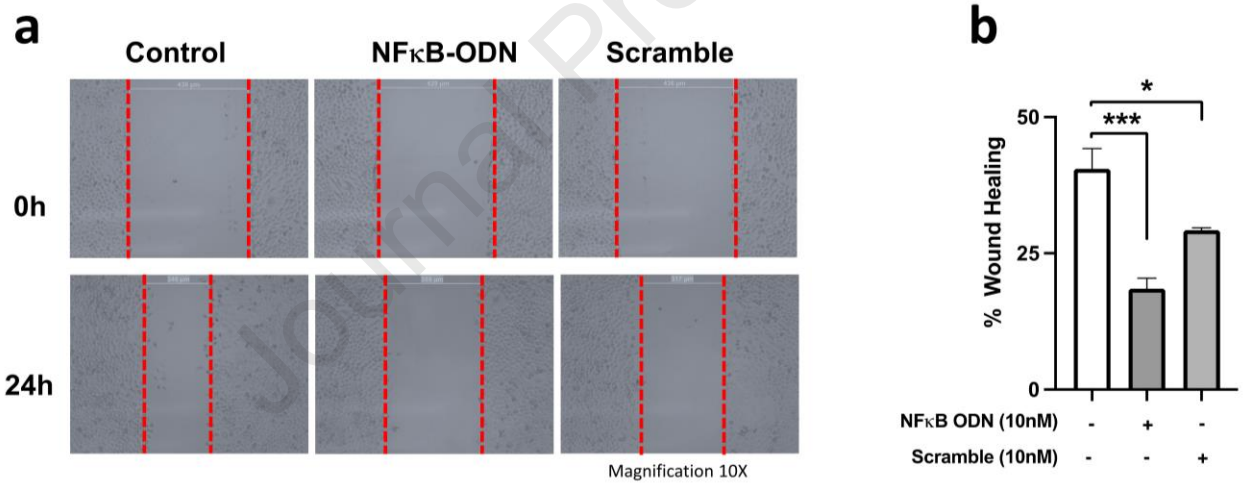

Figure 6. Anti-migratory activity by wound healing migration assay. *The wound was created by scratching, with a sterile pipette tip, a confluent layer of A549 cells. Cells were then treated with 10 nM Dex(NFκB-ODN) NPs or concentration-matched Dex(scrambled-ODN) NPs for 24 h. Photographs were acquired on a light microscope under 10x magnification (a). The distance between the edges of the wounds was measured before treatment (0 h) and after 24 h to calculate the percent wound closure (b). Values are expressed as average ± SEM of n = 3 independent experiments. Statistical analysis was performed by ordinary one-way ANOVA test. * = P < 0.05; *** = P < 0.001 vs control (untreated).*

A similar anti-migratory activity of the Dex(NFκB-ODN) NPs was observed with the transwell chamber assay. In this experiment, the Dex(NFκB-ODN) NPs significantly inhibited A549 cells migration (**Figure** a) by 43.2% compared to the untreated control (**Figure** b), while upon treatment with Dex(Scrambled-ODN) NPs, no significant inhibition of cells migration was observed as shown in **Figure** b.

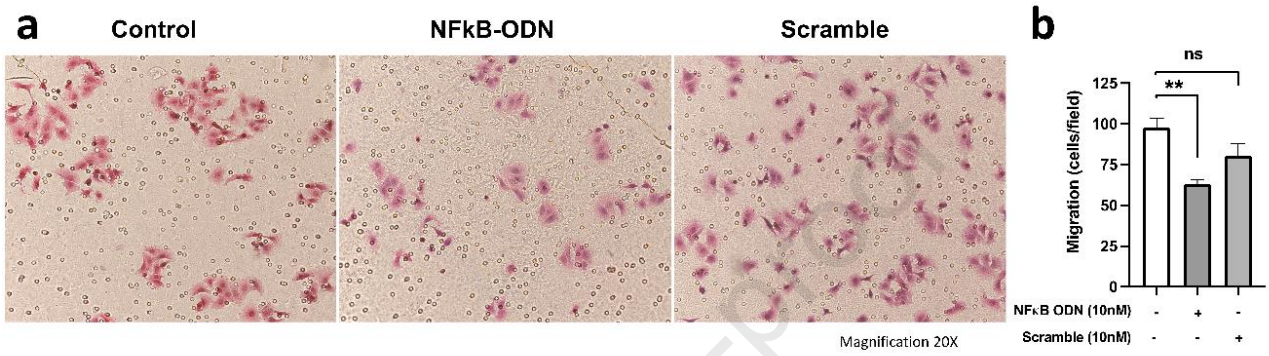

Figure 7. Anti-migratory activity of Dex(NFκB-ODN) NPs in A549 cells*: Transwell chamber assay. A549 cells were seeded in a transwell chamber previously coated with gelatin and treated with 10 nM Dex(NFκB-ODN) NPs or concentration-matched Dex(scrambled-ODN)NPs for 24 h. Subsequently, cells were allowed to migrate through the membrane for additional 24 h. The cells that successfully migrated were then stained with hematoxylin-eosin and imaged under a light microscope (a). The migrated cells were counted in 5 random positions per well under a high-power field (b). Values are expressed as average ± SEM of n = 3 independent experiments. Statistical analysis was performed by ordinary one-way ANOVA test. ns = P ≥ 0.05; ** = P < 0.01 vs control (untreated).*

3.8 Anti-Colony Formation Activity of NFκB-ODN-NPs in A549 Cells

The anti-colony formation activity of the Dex(NFκB-ODN) NPs in A549 cells was evaluated by colony formation assay after staining with crystal violet. The result of this assay is depicted in **Figure** , where the Dex(NFκB-ODN) NPs is shown to inhibit colony formation compared to the untreated and Dex(scrambled-ODN) NPs treated cells (**Figure** a). In particular, treatment with the Dex(NFκB-ODN) NPs resulted in a significantly high inhibition of colony formation up to 42% (**Figure** b).

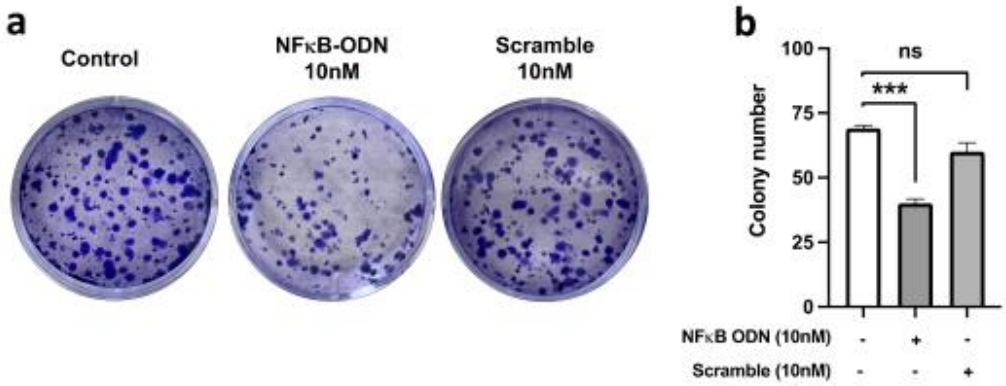

565

566 ***Figure 8. Anti-colony formation activity of Dex(NFκB-ODN) NPs in A549 cells.*** *A549 cells*
567 *were seeded at low density in 6-well plates and, after adhesion, treated with 10 nM Dex(NFκB-*
568 *ODN) NPs or concentration-matched Dex(scrambled-ODN) NPs for 24 h. After colony*
569 *formation (≈ 2 weeks), cells were stained with crystal violet solution and each individual well*
570 *was imaged using the light microscope (a). The resulting number of colonies in each well has*
571 *been counted and is plotted in (b). Values are expressed as average ± SEM of n = 3 independent*
572 *experiments. Statistical analysis was performed by ordinary one-way ANOVA test. ns = P ≥*
573 *0.05; ** = P < 0.01 vs control (untreated).*

574

4. Discussion

In this study, we have shown the potent anticancer activity of a SpAcDex-based NFκB decoy ODN formulations against an established *in vitro* model of lung cancer, the A549 NSCLC cell line. This anticancer activity was exerted primarily through the inhibition of proliferation, migration, and colony formation.

Both scrambled and NFκB decoy ODNs were encapsulated into an acid responsive SpAcDex NPs. The spermine-modified acetalated dextran material was synthesized according to *Cohen et al.* [46] The acetal modification of dextran introduces an acid-sensitive functional group to switch the solubility of dextran from hydrophilic to hydrophobic, allowing particle formulation using the emulsion method [49, 65]. These acetalated dextran-based nanocarriers have been effectively used for the delivery of a range of different payloads, including plasmid DNA [66]. To further improve the encapsulation efficiency for small oligonucleotides like siRNA or mRNA, the possibility of additional electrostatic interactions with the phosphate backbone of the RNAs, which is predicted to be exposed on the external surface of dsRNA strands, was provided via functionalization with cationic amines by introducing spermine molecules in the dextran backbone. The spermine modification resulted in an excellent loading of oligonucleotides. The presence of positive charges on the surface of SpAcDex NPs also enhances cellular uptake by improving their interaction with negatively charged cell membranes.

For the particle formulation and ODN encapsulation in spermine-modified acetalated dextran NPs, a double emulsion method was applied [67, 68]. The hydrophilic double-stranded decoy ODN dissolved in PBS buffer was added on top of the DCM layer containing spermine-modified acetalated dextran before the first sonication step to encapsulate this hydrophilic payload into the core of the NPs.

After secondary emulsion and solvent evaporation, narrow size distributed nanoparticles were obtained. The free decoy ODN was quantified by analysing the supernatant after centrifugation using a fluorescence-based indirect method with RiboGreen assay. This confirmed the successful encapsulation of decoy ODN in the nanoparticles. A high encapsulation efficiency was observed, which can be attributed to the electrostatic interaction between the cationic component of spermine AcDex material and the negatively charged decoy ODN [46].

The degradation of particles after incubation in acidic conditions was observed as a result of the hydrolysis of acetal groups. This process led to the conversion of the polysaccharide

component of the particles back to its water-soluble native form which ultimately leads to particle degradation. The pH-dependence of particle degradation was confirmed using dynamic light scattering (DLS) and visual observations over different time periods. Additionally, the release rate of oligonucleotide (ODN) from loaded particles was determined to be dependent on the pH, with a higher rate of release observed in acidic conditions. The observation of limited decoy ODN released under neutral pH 7.4 over a 24 h period acts as a control and highlights the stability of these particles in normal physiological conditions. This stability is critical for ensuring that the particles remain intact to avoid any unwanted leakage and the protection of loaded decoy ODN from nuclease activity in physiological environments such as the bloodstream or typical extracellular spaces, where neutral pH levels are maintained.

Additionally, these particles have been reported to escape endosomes upon cellular uptake via the proton sponge effect, due to the presence of amine content. Upon endocytosis, the degradation of these particles is triggered by low pH in the endosomal compartment. Furthermore, the buffering of the endosome by spermine content leads to accumulation of counterions (such as Cl^-), which raises the osmotic pressure and causes the endosome to burst [69, 70]. This releases the decoy ODN into the cytoplasm, protecting it from degradation by lysosomal enzymes and ensuring its successful delivery [71].

The overall stability of the particles under physiological conditions reduces the risk of unintended side effects and toxicity, while the acid-triggered release pattern suggests that decoy ODN will only be released in the acidic environment of tumor or endosome/lysosome, which makes this system an attractive candidate for administration of decoy oligonucleotides. The controlled release of decoy ODN from these particles may lead to improved therapeutic outcomes for patients. Next, we tested the anticancer activity of the Dex(NFκB-ODN) NPs formulation against A549 cells. We used A549 cells as an *in vitro* model of NSCLC as this cell line has been extensively characterized and is commonly used in NSCLC studies aimed at investigating mechanisms of action and efficacy of novel experimental anticancer drugs. In particular, the A549 cells are hypotriploid human alveolar basal epithelial cells, with extensive applications as *in vitro* model for lung adenocarcinoma and type II pulmonary epithelial cells [72]. Being cell proliferation and migration/metastasis two hallmarks of cancer progression [73, 74], we have investigated these processes in A549 cells by measuring the impact of treatment with Dex(NFκB-ODN) NPs on the cell ability to proliferate, migrate and form colonies.

As shown by the MTT assay, treatment with Dex(NFκB-ODN) NPs significantly inhibited (37.2%) the proliferation of A549 cells in a dose-dependent manner. Furthermore, we have obtained a low (12%), but significant, anti-proliferative activity when treating A549 cells with the 10 nM concentrated Dex(scrambled-ODN) NPs (here 10 nM concentration represents the concentration of ODNs). Considering that this anti-proliferative activity was sensibly lower compared to the value obtained with the concentration-matched Dex(NFκB-ODN) NPs, we performed the subsequent experiments using 10 nM concentrated ODNs. Furthermore, the fact that the anti-proliferative effect with the 10 nM concentrated Dex(scrambled-ODN) NPs was lower compared to the 10 nM Dex(NFκB-ODN) NPs, confirming that the anti-proliferative activity of the Dex(NFκB-ODN) NPs derives specifically from their NFκB-inhibiting action.

To assess the safety of the Dex(NFκB-ODN) NPs, the formulations were tested on non-cancerous BEAS-2B human bronchial epithelial cells. Although Dex(NFκB-ODN) NPs exerted a significant reduction of BEAS-2B cell viability, the relative safety of our formulation is demonstrated by the fact that, at the highest concentrations tested, the impact on BEAS-2B cell viability was significantly lower compared to the impact on A549 cell viability. This suggests that Dex(NFκB-ODN) NPs specifically inhibit the proliferation of cancerous A549 cells.

To assess whether the materials used in the synthesis of the NPs had any toxic effects on cells, empty nanoparticle were tested on both A549 and BEAS-2B cells. Treatment with empty NPs concentrations of up to 20 μg/mL resulted in no significant reduction of cell viability on both cell lines, in accordance with reports showing that the NPs materials have minimal toxicity against most cells at moderate concentrations [46].

Considering that, in PC-3M androgen-independent prostate cancer cells, the transfection with an NFκB decoy ODN has been reported to induce apoptosis, together with strong suppression of cell proliferation [32], we cannot exclude that, in our experiment, an eventual induction of apoptosis or necroptosis caused by NFκB blockade has at least a partial influence on the reduced metabolic activity reported by the MTT assay. To test this hypothesis, we have assessed the effect of Dex(NFκB-ODN) NPs on the expression of the genes RIPK1, MLKL, TNF-α, and RIPK3, which are collectively considered key mediators of apoptosis and necroptosis [75]. Treatment of A549 cells with Dex(NFκB-ODN) NPs resulted in an overall

increased expression of these genes, which reached statistical significance for RIPK1 and MLKL. The fact that Dex(NFκB-ODN) NPs induced a trend of increase of the expression of TNF-α and RIPK3 genes is caused by a relatively higher variability of the expression of these genes. However, these results collectively confirm that at least part of the anti-proliferative effect of Dex(NFκB-ODN) NPs is caused by the activation of the TNF-α/RIPK1/RIPK3/MLKL pathway which leads to necroptosis.

Furthermore, the inhibition of the NFκB pathway through treatment with the decoy ODN NPs exerted a significant anti-migratory activity, as demonstrated in the wound healing assay as well as in the transwell chamber assay. In the wound healing assay, treatment with Dex(scrambled-ODN) NPs exerted a slight anti-migratory activity, similar to what was observed in the MTT assay. However, a significantly stronger anti-migratory activity was obtained upon treatment with Dex(NFκB-ODN) NPs, which suggests this effect is exerted specifically through the inhibition of NFκB.

The anticancer activity of the Dex(NFκB-ODN) NPs was also supported by the colony formation assay, where a significantly lower number of colonies was formed upon treatment with Dex(NFκB-ODN) NPs compared to Dex(scrambled-ODN) NPs.

Taken together, these results underscore the strong anticancer activity of Dex(NFκB-ODN) NPs, further highlighting the therapeutic potential of NFκB blockage through NP-mediated delivery of decoy ODNs for lung cancer [27, 76].

The robustness and relevance of such a treatment approach would enormously benefit from a mechanistic explanation of the pathways through which the Dex(NFκB-ODN) NPs exert their anti-migratory activity. In the modified Boyden's chamber assay, the surface of the chamber was coated with 2.5% gelatin. Considering that gelatin is degraded by matrix metalloproteinases (MMPs) [77], it can be hypothesized that the reduction of the migratory ability of A549 cells obtained upon NFκB inhibition could be caused by the downregulation of MMPs expression and/or activity. This would also be in agreement with the fact that MMPs, including MMP2 and MMP9, are upregulated upon NFκB activation [78]. Therefore, the assessment of the levels of MMPs via Western blot [58], and/or of their activity through gel zymography [79], could shed further light on the mechanism by which the inhibition of NFκB signalling results in impaired migrating ability. A limitation of our study resides in the fact that only one cell line, A549, has been used to investigate the anticancer activity of Dex(NFκB-ODN) NPs. Although this cell line is a well-established model of LC [72], testing the anticancer

activity of Dex(NFκB-ODN) NPs on further human LC cell lines, as well as on animal models of LC, would surely deepen our comprehension of the exact mechanism(s) by which treatment with Dex(NFκB-ODN) NPs exerts its anticancer activity. This would also be useful in expanding the applicability of this treatment strategy against different subtypes of LC, as well as against other types of cancer, thus strongly enhancing its potential therapeutic range.

A point of strength of the present study lies in the great potential for clinical translation of the Dex(NFκB-ODN) NPs. Acetalated dextran, in fact, is an easy-to-synthesize, bio-compatible material derived by the FDA-approved dextran [80], and it is characterised by extreme versatility and tunability of application as drug delivery system [44, 65]. The application of Dex(NFκB-ODN) NPs in the treatment of lung diseases such as NSCLC is advantageous due to the possibility of deliver the therapeutic agent via inhalational delivery, which represents a privileged administration route for the direct delivery of drug to the lung tissue. Acetalated dextran nanoparticles are suitable for this application, as they can be formulated as dry powder to be administered via inhalation [46, 66, 80]. The *in vivo* study of the delivery and efficacy of Dex(NFκB-ODN) NPs would enormously streamline the clinical translation of this formulation.

5. Conclusions

In conclusion, this study strongly supports the feasibility of inhibiting the NFκB signalling pathway as a therapeutic approach against NSCLC using a cationic dextran-based pH-sensitive delivery system for decoy ODNs. An excellent loading and a controlled release of decoy ODN demonstrated the significance of polysaccharide-based NPs as a novel therapeutic strategy. This resulted in a strong, significant inhibition of three cancer hallmarks: cell proliferation, migration and colony formation. The results of this study provide an innovative direction into the clinical management of lung cancer. Furthermore, these findings represent a blueprint for further medical research and application against lung infectious diseases and other chronic respiratory diseases, providing solid theoretical bases to test similar nanoformulation approaches to enhance the pulmonary delivery of compounds with poor pharmacokinetic properties and bioavailability such as ODNs.

Declaration of interest: none

733

734 **Acknowledgments**

735 The authors are thankful to the Graduate School of Health, University of Technology Sydney,
736 Australia. KD is supported by a project grant from the Rebecca L Cooper Medical Research
737 Foundation and the Maridulu Budyari Gumal Sydney Partnership for Health, Education,
738 Research and Enterprise(SPHERE) RSEOH CAG Seed grant, fellowship and extension grant;
739 Faculty of Health MCR/ECR Mentorship Support Grant and UTS Global Strategic
740 Partnerships Seed Funding Scheme. GDR is supported by the UTS International Research
741 Scholarship and the UTS President's Scholarship. KRP is supported by a fellowship from
742 Prevent Cancer Foundation (PCF) and the International Association for the Study of Lung
743 Cancer (IASLC). We also thank Maryam Hosseini for her help with SEM imaging.

744

References

1. Sung H, Ferlay J, Siegel RL *et al*. Global Cancer Statistics 2020: GLOBOCAN Estimates of Incidence and Mortality Worldwide for 36 Cancers in 185 Countries. *CA Cancer J Clin* 71(3), 209-249 (2021).
2. Malyla V, Paudel KR, Shukla SD *et al*. Recent advances in experimental animal models of lung cancer. *Future Med Chem* 12(7), 567-570 (2020).
3. Wong MCS, Lao XQ, Ho KF, Goggins WB, Tse SLA. Incidence and mortality of lung cancer: global trends and association with socioeconomic status. *Sci Rep* 7(1), 14300 (2017).
4. Sharma P, Mehta M, Dhanjal DS *et al*. Emerging trends in the novel drug delivery approaches for the treatment of lung cancer. *Chem Biol Interact* 309 108720 (2019).
5. Onaitis MW, Petersen RP, Balderson SS *et al*. Thoracoscopic lobectomy is a safe and versatile procedure: experience with 500 consecutive patients. *Ann Surg* 244(3), 420-425 (2006).
6. Klastersky J, Awada A. Milestones in the use of chemotherapy for the management of non-small cell lung cancer (NSCLC). *Crit Rev Oncol Hematol* 81(1), 49-57 (2012).
7. Kang TM, Hardcastle N, Singh AK *et al*. Practical considerations of single-fraction stereotactic ablative radiotherapy to the lung. *Lung Cancer* 170 185-193 (2022).
8. Liu SY, Liu SM, Zhong WZ, Wu YL. Targeted Therapy in Early Stage Non-small Cell Lung Cancer. *Curr Treat Options Oncol* doi:10.1007/s11864-022-00994-w (2022).
9. Baci D, Cekani E, Imperatori A, Ribatti D, Mortara L. Host-Related Factors as Targetable Drivers of Immunotherapy Response in Non-Small Cell Lung Cancer Patients. *Front Immunol* 13 914890 (2022).
10. Paudel KR, Panth N, Pangeni R *et al*. Chapter 23 - Targeting lung cancer using advanced drug delivery systems. In: *Targeting Chronic Inflammatory Lung Diseases Using Advanced Drug Delivery Systems*, Dua K,Hansbro PM,Wadhwa R,Haghi M,Pont LG,Williams KA (Ed.^(Eds).Academic Press 493-516 (2020).
11. Yazbeck V, Alesi E, Myers J, Hackney MH, Cuttino L, Gewirtz DA. An overview of chemotoxicity and radiation toxicity in cancer therapy. *Adv Cancer Res* 155 1-27 (2022).
12. Paudel KR, Chellappan DK, Macloughlin R, Pinto TJA, Dua K, Hansbro PM. Editorial: Advanced therapeutic delivery for the management of chronic respiratory diseases. *Front Med (Lausanne)* 9 983583 (2022).
13. Paudel KR, Dua K, Panth N, Hansbro PM, Chellappan DK. Advances in research with rutin-loaded nanoformulations in mitigating lung diseases. *Future Med Chem* 14(18), 1293-1295 (2022).
14. Malyla V, Paudel KR, Rubis GD, Hansbro NG, Hansbro PM, Dua K. Extracellular Vesicles Released from Cancer Cells Promote Tumorigenesis by Inducing Epithelial to Mesenchymal Transition via β-Catenin Signaling. *International Journal of Molecular Sciences* 24(4), 3500 (2023).
15. Sen R, Baltimore D. In vitro transcription of immunoglobulin genes in a B-cell extract: effects of enhancer and promoter sequences. *Mol Cell Biol* 7(5), 1989-1994 (1987).
16. Zhang Q, Lenardo MJ, Baltimore D. 30 Years of NF-κB: A Blossoming of Relevance to Human Pathobiology. *Cell* 168(1-2), 37-57 (2017).
17. Xia L, Tan S, Zhou Y *et al*. Role of the NFκB-signaling pathway in cancer. *Onco Targets Ther* 11 2063-2073 (2018).

18. Taniguchi K, Karin M. NF-κB, inflammation, immunity and cancer: coming of age. *Nat Rev Immunol* 18(5), 309-324 (2018).
19. Cai Z, Tchou-Wong KM, Rom WN. NF-kappaB in lung tumorigenesis. *Cancers (Basel)* 3(4), 4258-4268 (2011).
20. Jones DR, Broad RM, Madrid LV, Baldwin AS, Jr., Mayo MW. Inhibition of NF-kappaB sensitizes non-small cell lung cancer cells to chemotherapy-induced apoptosis. *Ann Thorac Surg* 70(3), 930-936; discussion 936-937 (2000).
21. Gao M, Yeh PY, Lu YS, Chang WC, Kuo ML, Cheng AL. NF-kappaB p50 promotes tumor cell invasion through negative regulation of invasion suppressor gene CRMP-1 in human lung adenocarcinoma cells. *Biochem Biophys Res Commun* 376(2), 283-287 (2008).
22. Kumar M, Allison DF, Baranova NN *et al*. NF-κB regulates mesenchymal transition for the induction of non-small cell lung cancer initiating cells. *PLoS One* 8(7), e68597 (2013).
23. Gu L, Wang Z, Zuo J, Li H, Zha L. Prognostic significance of NF-κB expression in non-small cell lung cancer: A meta-analysis. *PLoS One* 13(5), e0198223 (2018).
24. Wong KK, Jacks T, Dranoff G. NF-kappaB fans the flames of lung carcinogenesis. *Cancer Prev Res (Phila)* 3(4), 403-405 (2010).
25. Yu H, Lin L, Zhang Z, Zhang H, Hu H. Targeting NF-κB pathway for the therapy of diseases: mechanism and clinical study. *Signal Transduct Target Ther* 5(1), 209 (2020).
26. Ramadass V, Vaiyapuri T, Tergaonkar V. Small Molecule NF-κB Pathway Inhibitors in Clinic. *Int J Mol Sci* 21(14), (2020).
27. Mehta M, Paudel KR, Shukla SD *et al*. Recent trends of NFκB decoy oligodeoxynucleotide-based nanotherapeutics in lung diseases. *J Control Release* 337 629-644 (2021).
28. Wardwell PR, Bader RA. Immunomodulation of cystic fibrosis epithelial cells via NF-kappaB decoy oligonucleotide-coated polysaccharide nanoparticles. *J Biomed Mater Res A* 103(5), 1622-1631 (2015).
29. Ahmad MZ, Akhter S, Mallik N, Anwar M, Tabassum W, Ahmad FJ. Application of decoy oligonucleotides as novel therapeutic strategy: a contemporary overview. *Curr Drug Discov Technol* 10(1), 71-84 (2013).
30. Mann MJ. Transcription factor decoys: a new model for disease intervention. *Ann N Y Acad Sci* 1058 128-139 (2005).
31. Imran M, Jha LA, Hasan N *et al*. "Nanodecoys" - Future of drug delivery by encapsulating nanoparticles in natural cell membranes. *Int J Pharm* 621 121790 (2022).
32. Fang Y, Sun H, Zhai J *et al*. Antitumor activity of NF-kB decoy oligodeoxynucleotides in a prostate cancer cell line. *Asian Pac J Cancer Prev* 12(10), 2721-2726 (2011).
33. Morishita R, Higaki J, Tomita N, Ogihara T. Application of transcription factor "decoy" strategy as means of gene therapy and study of gene expression in cardiovascular disease. *Circ Res* 82(10), 1023-1028 (1998).
34. Dinh TD, Higuchi Y, Kawakami S, Yamashita F, Hashida M. Evaluation of osteoclastogenesis via NFkappaB decoy/mannosylated cationic liposome-mediated inhibition of pro-inflammatory cytokine production from primary cultured macrophages. *Pharm Res* 28(4), 742-751 (2011).
35. De Stefano D. Oligonucleotides decoy to NF-kappaB: becoming a reality? *Discov Med* 12(63), 97-105 (2011).

36. Farahmand L, Darvishi B, Majidzadeh AK. Suppression of chronic inflammation with engineered nanomaterials delivering nuclear factor κB transcription factor decoy oligodeoxynucleotides. *Drug Deliv* 24(1), 1249-1261 (2017).
37. Mischiati C, Borgatti M, Bianchi N *et al*. Interaction of the human NF-kappaB p52 transcription factor with DNA-PNA hybrids mimicking the NF-kappaB binding sites of the human immunodeficiency virus type 1 promoter. *J Biol Chem* 274(46), 33114-33122 (1999).
38. Crinelli R, Bianchi M, Gentilini L *et al*. Transcription factor decoy oligonucleotides modified with locked nucleic acids: an in vitro study to reconcile biostability with binding affinity. *Nucleic Acids Res* 32(6), 1874-1885 (2004).
39. Farahmand L, Darvishi B, Majidzadeh AK. Suppression of chronic inflammation with engineered nanomaterials delivering nuclear factor kappaB transcription factor decoy oligodeoxynucleotides. *Drug Deliv* 24(1), 1249-1261 (2017).
40. Doroudian M, Macloughlin R, Poynton F, Prina-Mello A, Donnelly SC. Nanotechnology based therapeutics for lung disease. *Thorax* 74(10), 965-976 (2019).
41. De Rosa G, Maiuri MC, Ungaro F *et al*. Enhanced intracellular uptake and inhibition of NF-kappaB activation by decoy oligonucleotide released from PLGA microspheres. *J Gene Med* 7(6), 771-781 (2005).
42. De Stefano D, De Rosa G, Maiuri MC *et al*. Oligonucleotide decoy to NF-kappaB slowly released from PLGA microspheres reduces chronic inflammation in rat. *Pharmacol Res* 60(1), 33-40 (2009).
43. Zhang N, Wardwell PR, Bader RA. Polysaccharide-based micelles for drug delivery. *Pharmaceutics* 5(2), 329-352 (2013).
44. Prasher P, Sharma M, Mehta M *et al*. Current-status and applications of polysaccharides in drug delivery systems. *Colloid and Interface Science Communications* 42 100418 (2021).
45. Ma L, Shen CA, Gao L *et al*. Anti-inflammatory activity of chitosan nanoparticles carrying NF-kappaB/p65 antisense oligonucleotide in RAW264.7 macropghage stimulated by lipopolysaccharide. *Colloids Surf B Biointerfaces* 142 297-306 (2016).
46. Cohen JL, Schubert S, Wich PR *et al*. Acid-degradable cationic dextran particles for the delivery of siRNA therapeutics. *Bioconjug Chem* 22(6), 1056-1065 (2011).
47. Boedtkjer E, Pedersen SF. The Acidic Tumor Microenvironment as a Driver of Cancer. *Annu Rev Physiol* 82 103-126 (2020).
48. Bachelder EM, Beaudette TT, Broaders KE, Dashe J, Frechet JM. Acetal-derivatized dextran: an acid-responsive biodegradable material for therapeutic applications. *J Am Chem Soc* 130(32), 10494-10495 (2008).
49. Wang S, Fontana F, Shahbazi MA, Santos HA. Acetalated dextran based nano- and microparticles: synthesis, fabrication, and therapeutic applications. *Chem Commun (Camb)* 57(35), 4212-4229 (2021).
50. Bamberger D, Hobernik D, Konhauser M, Bros M, Wich PR. Surface Modification of Polysaccharide-Based Nanoparticles with PEG and Dextran and the Effects on Immune Cell Binding and Stimulatory Characteristics. *Mol Pharm* 14(12), 4403-4416 (2017).
51. Shi K, Xue J, Fang Y *et al*. Inorganic Kernel-Reconstituted Lipoprotein Biomimetic Nanovehicles Enable Efficient Targeting "Trojan Horse" Delivery of STAT3-Decoy Oligonucleotide for Overcoming TRAIL Resistance. *Theranostics* 7(18), 4480-4497 (2017).
52. Centelles MN, Qian C, Campanero MA, Irache JM. New methodologies to characterize the effectiveness of the gene transfer mediated by DNA-chitosan nanoparticles. *Int J Nanomedicine* 3(4), 451-460 (2008).

53. Hanwell MD, Curtis DE, Lonie DC, Vandermeersch T, Zurek E, Hutchison GR. Avogadro: an advanced semantic chemical editor, visualization, and analysis platform. *Journal of Cheminformatics* 4(1), 17 (2012).
54. Pettersen EF, Goddard TD, Huang CC *et al*. UCSF Chimera—A visualization system for exploratory research and analysis. *Journal of Computational Chemistry* 25(13), 1605-1612 (2004).
55. Lee HH, Paudel KR, Kim DW. Terminalia chebula Fructus Inhibits Migration and Proliferation of Vascular Smooth Muscle Cells and Production of Inflammatory Mediators in RAW 264.7. *Evid Based Complement Alternat Med* 2015 502182 (2015).
56. Paudel KR, Panth N, Manandhar B *et al*. Attenuation of Cigarette-Smoke-Induced Oxidative Stress, Senescence, and Inflammation by Berberine-Loaded Liquid Crystalline Nanoparticles: In Vitro Study in 16HBE and RAW264.7 Cells. *Antioxidants (Basel)* 11(5), (2022).
57. Jun MY, Karki R, Paudel KR, Sharma BR, Adhikari D, Kim DW. Alkaloid rich fraction from Nelumbo nucifera targets VSMC proliferation and migration to suppress restenosis in balloon-injured rat carotid artery. *Atherosclerosis* 248 179-189 (2016).
58. Paudel KR, Wadhwa R, Tew XN *et al*. Rutin loaded liquid crystalline nanoparticles inhibit non-small cell lung cancer proliferation and migration in vitro. *Life Sci* 276 119436 (2021).
59. Paudel KR, Mehta M, Yin GHS *et al*. Berberine-loaded liquid crystalline nanoparticles inhibit non-small cell lung cancer proliferation and migration in vitro. *Environ Sci Pollut Res Int* 29(31), 46830-46847 (2022).
60. Wadhwa R, Paudel KR, Chin LH *et al*. Anti-inflammatory and anticancer activities of Naringenin-loaded liquid crystalline nanoparticles in vitro. *J Food Biochem* 45(1), e13572 (2021).
61. Alnuqaydan AM, Almutary AG, Azam M *et al*. Evaluation of the Cytotoxic Activity and Anti-Migratory Effect of Berberine-Phytantriol Liquid Crystalline Nanoparticle Formulation on Non-Small-Cell Lung Cancer In Vitro. *Pharmaceutics* 14(6), (2022).
62. Wan L, Yao X, Faiola F *et al*. Coating with spermine-pullulan polymer enhances adenoviral transduction of mesenchymal stem cells. *Int J Nanomedicine* 11 6763-6769 (2016).
63. Breitenbach BB, Steiert E, Konhäuser M *et al*. Double stimuli-responsive polysaccharide block copolymers as green macrosurfactants for near-infrared photodynamic therapy. *Soft Matter* 15(6), 1423-1434 (2019).
64. Braga CB, Perli G, Becher TB, Ornelas C. Biodegradable and pH-Responsive Acetalated Dextran (Ac-Dex) Nanoparticles for NIR Imaging and Controlled Delivery of a Platinum-Based Prodrug into Cancer Cells. *Mol Pharm* 16(5), 2083-2094 (2019).
65. Bachelder EM, Pino EN, Ainslie KM. Acetalated Dextran: A Tunable and Acid-Labile Biopolymer with Facile Synthesis and a Range of Applications. *Chem Rev* 117(3), 1915-1926 (2017).
66. Cohen JA, Beaudette TT, Cohen JL, Broaders KE, Bachelder EM, Frechet JM. Acetal-modified dextran microparticles with controlled degradation kinetics and surface functionality for gene delivery in phagocytic and non-phagocytic cells. *Adv Mater* 22(32), 3593-3597 (2010).
67. Foerster F, Bamberger D, Schupp J *et al*. Dextran-based therapeutic nanoparticles for hepatic drug delivery. *Nanomedicine* 11(20), 2663-2677 (2016).
68. Konhauser M, Kannaujiya VK, Steiert E, Schwickert K, Schirmeister T, Wich PR. Co-encapsulation of l-asparaginase and etoposide in dextran nanoparticles for synergistic effect in chronic myeloid leukemia cells. *Int J Pharm* 622 121796 (2022).

69. Nguyen J, Szoka FC. Nucleic acid delivery: the missing pieces of the puzzle? *Acc Chem Res* 45(7), 1153-1162 (2012).
70. Mahajan S, Tang T. Polyethylenimine-DNA Nanoparticles under Endosomal Acidification and Implication to Gene Delivery. *Langmuir* 38(27), 8382-8397 (2022).
71. Akinc A, Thomas M, Klibanov AM, Langer R. Exploring polyethylenimine-mediated DNA transfection and the proton sponge hypothesis. *J Gene Med* 7(5), 657-663 (2005).
72. Lieber M, Smith B, Szakal A, Nelson-Rees W, Todaro G. A continuous tumor-cell line from a human lung carcinoma with properties of type II alveolar epithelial cells. *Int J Cancer* 17(1), 62-70 (1976).
73. Wadhwa R, Paudel KR, Shukla S *et al*. Epigenetic Therapy as a Potential Approach for Targeting Oxidative Stress–Induced Non-small-Cell Lung Cancer. In: *Handbook of Oxidative Stress in Cancer: Mechanistic Aspects*, Chakraborti S,Ray BK,Roychoudhury S (Ed.^(Eds).Springer Nature Singapore Singapore 1545-1560 (2022).
74. Khursheed R, Dua K, Vishwas S *et al*. Biomedical applications of metallic nanoparticles in cancer: Current status and future perspectives. *Biomed Pharmacother* 150 112951 (2022).
75. Seo J, Nam YW, Kim S, Oh D-B, Song J. Necroptosis molecular mechanisms: Recent findings regarding novel necroptosis regulators. *Experimental & Molecular Medicine* 53(6), 1007-1017 (2021).
76. Dimitrakopoulos FD, Kottorou AE, Kalofonou M, Kalofonos HP. The Fire Within: NF-κB Involvement in Non-Small Cell Lung Cancer. *Cancer Res* 80(19), 4025-4036 (2020).
77. Mook OR, Van Overbeek C, Ackema EG, Van Maldegem F, Frederiks WM. In situ localization of gelatinolytic activity in the extracellular matrix of metastases of colon cancer in rat liver using quenched fluorogenic DQ-gelatin. *J Histochem Cytochem* 51(6), 821-829 (2003).
78. Li J, Lau GK, Chen L *et al*. Interleukin 17A promotes hepatocellular carcinoma metastasis via NF-kB induced matrix metalloproteinases 2 and 9 expression. *PLoS One* 6(7), e21816 (2011).
79. Frankowski H, Gu YH, Heo JH, Milner R, Del Zoppo GJ. Use of gel zymography to examine matrix metalloproteinase (gelatinase) expression in brain tissue or in primary glial cultures. *Methods Mol Biol* 814 221-233 (2012).
80. Prasher P, Sharma M, Kumar Singh S *et al*. Versatility of acetalated dextran in nanocarriers targeting respiratory diseases. *Materials Letters* 323 132600 (2022).

FIGURES CAPTIONS

Figure 1. Characterisation of decoy ODN-Encapsulated dextran NPs. *(a) Size distribution obtained by DLS; (b) SEM analysis.*

Figure 2. Particle degradation under pH 5.5 and pH 7.4 (a) DLS data; (b) visual observation

Figure 3. Decoy ODN release under pH 5.5 and pH 7.4 *(Data are presented as means ± SD (n = 3))*

Figure 4. Anti-proliferative activity by MTT assay*: The A549 cells (a-c) and BEAS-2B cells (d-f) were treated with various doses of Dex(NFκB-ODN) NPs (a, d) or Dex(scrambled-ODN) NPs (b, e) or empty NPs (c, f) for 24 hours. The values are expressed as average ± SEM of n = 3 independent experiments. Statistical analysis was performed by ordinary one-way ANOVA test. * = P < 0.05; ** = P < 0.01; **** = P < 0.0001 vs control (untreated). In (d), # = P<0.05 vs concentration-matched group on A549 cells as assessed by Mann-Whitney U test.*

Figure 5. Effect of Dex(NFκB-ODN) NPs on the expression of apoptosis/necroptosis genes in A549 cells. *A549 cells were treated with 10 nM Dex(NFκB-ODN) NPs or Dex(Scramble-ODN) NPs and the relative expression of the following genes was measured with real-time qPCR: RIPK1 (a), MLKL (b), TNF-α(c), and RIPK3 (d). Values are expressed as average ± SEM of n = 3 independent experiments. Statistical analysis was performed by ordinary one-way ANOVA test * = P < 0.05 vs control (untreated).*

Figure 6. Anti-migratory activity by wound healing migration assay. *The wound was created by scratching, with a sterile pipette tip, a confluent layer of A549 cells. Cells were then treated with 10 nM Dex(NFκB-ODN) NPs or concentration-matched Dex(scrambled-ODN) NPs for 24 h. Photographs were acquired on a light microscope under 10x magnification (a). The distance between the edges of the wounds was measured before treatment (0 h) and after 24 h to calculate the percent wound closure (b). Values are expressed as average ± SEM of n = 3*

*independent experiments. Statistical analysis was performed by ordinary one-way ANOVA test. * = P < 0.05; *** = P < 0.001 vs control (untreated).*

Figure 7. Anti-migratory activity of Dex(NFκB-ODN) NPs in A549 cells: Transwell chamber assay. *A549 cells were seeded in a transwell chamber previously coated with gelatin and treated with 10 nM Dex(NFκB-ODN) NPs or concentration-matched Dex(scrambled-ODN)NPs for 24 h. Subsequently, cells were allowed to migrate through the membrane for additional 24 h. The cells that successfully migrated were then stained with hematoxylin-eosin and imaged under a light microscope (a). The migrated cells were counted in 5 random positions per well under a high-power field (b). Values are expressed as average ± SEM of n = 3 independent experiments. Statistical analysis was performed by ordinary one-way ANOVA test. ns = P ≥ 0.05; ** = P < 0.01 vs control (untreated).*

Figure 8. Anti-colony formation activity of Dex(NFκB-ODN) NPs in A549 cells. *A549 cells were seeded at low density in 6-well plates and, after adhesion, treated with 10 nM Dex(NFκB-ODN) NPs or concentration-matched Dex(scrambled-ODN) NPs for 24 h. After colony formation (≈ 2 weeks), cells were stained with crystal violet solution and each individual well was imaged using the light microscope (a). The resulting number of colonies in each well has been counted and is plotted in (b). Values are expressed as average ± SEM of n = 3 independent experiments. Statistical analysis was performed by ordinary one-way ANOVA test. ns = P ≥ 0.05; ** = P < 0.01 vs control (untreated).*

Dr. Kamal Dua
Discipline of Pharmacy,
Graduate School of Health,
University of Technology Sydney,
NSW, Australia
Center for Inflammation,
Centenary Institute, NSW, Australia

Dr. Peter R Wich
School of Chemical Engineering, University of New South Wales, Sydney, NSW 2052, Australia
Australian Centre for NanoMedicine,
University of New South Wales, Sydney, NSW 2052, Australia

20th November 2022

The Editor-in-Chief, Journal of Drug Delivery Science and Technology

The authors of the manuscript entitled **"Anticancer activity of NFκB decoy oligonucleotide-loaded nanoparticles against human lung adenocarcinoma"**, submitted for consideration for publication in the *Journal of Drug Delivery Science and Technology*, confirm that there are no interests to declare.

Kind regards,

Dr. Kamal Dua
Dr. Peter R Wich

Author	Role
Vinod Kumar Kannaujiya	Conceptualization Data curation Formal analysis Investigation Methodology Writing – review & editing
Gabriele De Rubis	Conceptualization Data Curation Formal Analysis Investigation Writing – original draft Writing – review & editing
Keshav Raj Paudel	Data curation Formal analysis Investigation Methodology Writing – review & editing
Bikash Manandhar	Data curation Formal analysis Investigation Methodology Writing – review & editing
Dinesh Kumar Chellappan	Methodology
Sachin Kumar Singh	Methodology
Ronan MacLoughlin	Resources Methodology
Gaurav Gupta	Methodology
Dia Xenaki	Methodology
Pradeep Kumar	Data curation Formal analysis Investigation Methodology
Philip Michael Hansbro	Supervision
Brian Gregory George Oliver	Conceptualization Supervision
Peter Richard Wich	Supervision Resources Conceptualization Funding acquisition Methodology Project Administration Writing – review & editing
Kamal Dua	Supervision Resources Conceptualization Funding acquisition Methodology Project Administration Writing – review & editing